



HAL
open science

Mice with humanized livers reveal the involvement of hepatocyte circadian clocks in rhythmic behavior and physiology

Anne-Sophie Delbès, Mar Quiñones, Cédric Gobet, Julien Castel, Raphaël Denis, Jérémy Berthelet, Benjamin Weger, Etienne Challet, Aline Charpagne, Sylviane Metairon, et al.

► **To cite this version:**

Anne-Sophie Delbès, Mar Quiñones, Cédric Gobet, Julien Castel, Raphaël Denis, et al.. Mice with humanized livers reveal the involvement of hepatocyte circadian clocks in rhythmic behavior and physiology. 2022. hal-03835781

HAL Id: hal-03835781

<https://hal.science/hal-03835781v1>

Preprint submitted on 1 Nov 2022

HAL is a multi-disciplinary open access archive for the deposit and dissemination of scientific research documents, whether they are published or not. The documents may come from teaching and research institutions in France or abroad, or from public or private research centers.

L'archive ouverte pluridisciplinaire **HAL**, est destinée au dépôt et à la diffusion de documents scientifiques de niveau recherche, publiés ou non, émanant des établissements d'enseignement et de recherche français ou étrangers, des laboratoires publics ou privés.

1 **Mice with humanized livers reveal the involvement of hepatocyte**
2 **circadian clocks in rhythmic behavior and physiology**

3
4 Anne-Sophie Delbès¹, Mar Quiñones^{1,2,3,15}, Cédric Gobet^{4,5,15}, Julien Castel¹, Raphaël G. P
5 Denis^{1,6}, Jérémy Berthelet⁷, Benjamin D. Weger^{4,8}, Etienne Challet⁹, Aline Charpagne⁴,
6 Sylviane Metairon⁴, Julie Piccand⁴, Marine Kraus⁴, Bettina H. Rohde¹⁰, John Bial¹¹, Elizabeth
7 M. Wilson¹², Lise-Lotte Vedin¹³, Mirko E. Minniti¹³, Matteo Pedrelli^{13,14}, Paolo Parini^{13,14},
8 *Frédéric Gachon^{4,5,8,16} & *Serge Luquet^{1,16,17}

9
10 ¹ Université Paris Cité, BFA, UMR 8251, CNRS, F-75013 Paris, France.

11 ² Instituto de Investigación Sanitaria de Santiago de Compostela, Complejo Hospitalario
12 Universitario de Santiago (CHUS/SERGAS), Travesía da Choupana s/n, 15706 Santiago de
13 Compostela, Spain

14 ³ CIBER de Fisiopatología de la Obesidad y la Nutrición (CIBEROBN), Instituto de Salud
15 Carlos III, 28029, Madrid, Spain.

16 ⁴ Nestlé Research, Société des Produits Nestlé, CH-1015 Lausanne, Switzerland

17 ⁵ School of Life Sciences, Ecole Polytechnique Fédérale de Lausanne, CH-1015 Lausanne,
18 Switzerland

19 ⁶ Institut Cochin, Université Paris Cité, INSERM U1016, CNRS UMR 8104, 75014 Paris,
20 France

21 ⁷ Université Paris Cité, CNRS, Unité Epigenétique et Destin Cellulaire, F-75013 Paris,
22 France.

23 ⁸ Institute for Molecular Bioscience, The University of Queensland, QLD-4072 St. Lucia,
24 Australia

25 ⁹ Institute for Cellular and Integrative Neurosciences, CNRS and University of Strasbourg,
26 Strasbourg, France

27 ¹⁰ Eurofins Genomics Europe Sequencing GmbH, European Genome and Diagnostics
28 Centre, Konstanz, Germany

29 ¹¹ Capsigen, Inc., Vancouver, WA, United States of America

30 ¹² Yecuris Corporation, Portland, Oregon, United States of America

31 ¹³ Cardio Metabolic Unit, Department of Medicine and department of Laboratory Medicine,
32 Karolinska Institute, Huddinge, Sweden

33 ¹⁴ Medical Unit Endocrinology, Theme Inflammation and Ageing, Karolinska University
34 Hospital, Stockholm, Sweden

35 ¹⁵ co second authors

36 ¹⁶ co last authors

37 ¹⁷ Lead contact

38
39 *Correspondence : Serge Luquet: serge.luquet@u-paris.fr (SL), Frédéric Gachon (FG)

40 f.gachon@imb.uq.edu.au

41 Lead contact : Serge Luquet: serge.luquet@u-paris.fr (SL),

42

43

44 **ABSTRACT**

45

46 The circadian clock is an evolutionarily acquired gene network that synchronizes
47 physiological processes to adapt homeostasis to the succession of day and night. While
48 most mammalian cells have a circadian clock, their synchronization at the body-level
49 depends on a central pacemaker located in the suprachiasmatic nuclei of the hypothalamus
50 that integrates light signals. However, peripheral organs are also synchronized by feeding
51 cues that can uncoupled them from the central pacemaker. Nevertheless, the potential
52 feedback of peripheral signals on the central clock remains poorly characterized. To discover
53 whether peripheral organ circadian clocks may affect the central pacemaker, we used a
54 chimeric model in which mouse hepatocytes were replaced by human hepatocytes. These
55 human hepatocytes showed a specific rhythmic physiology caused by their blunted response
56 to mouse systemic signals. Strikingly, mouse liver humanization reprogrammed the liver
57 diurnal gene expression and modified the phase of the circadian clock. The phase advance
58 was also reflected in the muscle as well as the entire rhythmic physiology of the animals,
59 indicating an impact on the circadian function of the central clock. Like mice with a deficient
60 central clock, the humanized animals shifted their rhythmic physiology more rapidly to the
61 light phase under day feeding. Our results indicate that peripheral clocks may affect the
62 central pacemaker and offer new perspectives to understand the impact of peripheral clocks
63 on the global circadian physiology.

64

65 **INTRODUCTION**

66 To adapt homeostasis to the changing environment present on Earth, organisms from
67 bacteria to mammals have evolved a timing system that anticipates these changes. This
68 endogenous timing system, called the circadian clock, orchestrates most aspects of
69 physiology and behavior. The mammalian circadian system is hierarchically organized. A
70 central clock localized in the suprachiasmatic nucleus (SCN) of the hypothalamus is daily
71 synchronized by light via the retino-hypothalamic tract and coordinates the peripheral clocks
72 localized in peripheral tissues (Hastings et al., 2018). The SCN synchronizes most aspects of
73 circadian physiology and is required to keep phase coherence between the different
74 peripheral organs (Ralph et al., 1990; Sinturel et al., 2021; Yoo et al., 2004). Nonetheless,
75 how the SCN orchestrates this phase coherence is still only partially understood.

76 However, in the absence of SCN, the individual peripheral organs continue to show robust
77 rhythms, indicating the existence of self-sustained cellular clocks (Sinturel et al., 2021; Yoo
78 et al., 2004). In all mammalian cells, this rhythmicity is generated by a molecular machinery
79 consisting of interconnected transcriptional and translational feedback loops in which the
80 transcription factor Brain and Muscle Aryl hydrocarbon receptor nuclear translocator-Like 1
81 (BMAL1, encoded by the *Arntl* gene) plays a critical role (Patke et al., 2020). Abolishing
82 BMAL1 activity in mouse hepatocytes demonstrated that around 35% of liver rhythmic genes
83 depend on a functional circadian clock whereas the other rhythmic genes are regulated by
84 systemic and/or feeding cues (Johnson et al., 2014; Kornmann et al., 2007; Weger et al.,
85 2021). Nevertheless, disrupting hepatocyte clock has no impact on the central clock in the
86 SCN (Johnson et al., 2014; Lamia et al., 2008). On the other hand, restoring *Bmal1*
87 expression and a functional circadian clock in a full-body *Bmal1* knockout (KO) animal has
88 no effect on the global rhythmic activity and behavior of these animals (Koronowski et al.,
89 2019). Therefore, while the central clock synchronizes peripheral clocks, there is so far no
90 evidence that peripheral clocks can impact the central clock in the SCN.

91 Also, recent evidence further suggests that the circadian clocks of different cell types
92 communicate between each other inside the same organ. For example, astrocytes circadian
93 clock can entrain neuronal clock in the SCN (Brancaccio et al., 2019; Patton et al., 2022) and
94 is important to determine the circadian period (Barca-Mayo et al., 2017; Tso et al., 2017).
95 Moreover, the disruption of the circadian clock in hepatocytes modulates the rhythmic gene
96 expression of other liver cell types (Guan et al., 2020) and even the synchronization of the
97 circadian clock in other tissues in response to feeding cues (Manella et al., 2021). These
98 studies highlight the importance of the communication between the clocks in the different cell
99 types inside the same tissue or in other more distant tissues (Koronowski and Sassone-
100 Corsi, 2021).

101 To decipher further the impact of these cellular communications in the organization of liver
102 circadian physiology, we implanted in mouse liver human hepatocytes that are hypothesized
103 to show different physiological properties and responses to systemic and feeding cues
104 compared to mouse hepatocytes (Azuma et al., 2007; Jiang et al., 2020), as well as different
105 rhythmic functions as shown in non-human primates (Mure et al., 2018). Here we show that
106 implantation of human hepatocytes in mice (Liver Humanized Mice: LHM) result in a global
107 loss of rhythmicity in liver gene expression in comparison to control animals implanted with
108 mouse hepatocytes (Liver “Murinized” Mice: LMM). While most circadian clock genes were
109 still rhythmic in the liver of LHM, they displayed an advanced phase and lower amplitude in
110 both mouse and human hepatocytes, suggesting that human hepatocytes can entrain the
111 remaining mouse hepatocytes in the liver of LHM. Strikingly, we discovered that these
112 human hepatocytes also regulate rhythmic gene in the muscle and impact global rhythmic
113 behavior and metabolism, suggesting potential feedback of the implanted human
114 hepatocytes on the hypothalamus and the central clock in the SCN. Finally, during imposed
115 day feeding, LHM adapted more quickly to the light phase, confirming that the engrafted
116 human hepatocytes impacts the entrainment property of the central circadian pacemaker.
117 Altogether, the chimeric LHM provide a yet uncharacterized mechanism by which
118 perturbation of the liver clock might directly alter global circadian physiology.

119

120 RESULTS

121

122 Human hepatocytes in a rodent environment impose specific rhythmic gene 123 expression to surrounding liver cells

124 It is now established that most cells in the body contain self-sustained molecular clocks that
125 can be synchronized by both signals from the central clock in the SCN and systemic cues
126 including feeding rhythm (Atger et al., 2017; Koronowski and Sassone-Corsi, 2021).
127 Recently, it has been shown that the disruption of the circadian clock specifically in
128 hepatocyte (Guan et al., 2020; Manella et al., 2021) or the presence of a functional clock only
129 in hepatocyte in a clock-depleted animal (Greco et al., 2021; Koronowski et al., 2019)
130 modulate the rhythmic expression in other cell types inside the same tissue or in other
131 tissues, as well as their response to feeding. However, while transplanting SCN cells with
132 different circadian properties in an intact animal can transfer the donor's SCN circadian
133 properties and impact animal behavior (Ralph et al., 1990), there is no description of such
134 effects for peripheral tissues.

135 To answer this question, we used chimeric LHM in which mice livers are repopulated with
136 human hepatocytes that are expected to have their own circadian properties and capacities
137 to respond to systemic signals, as described for human and another diurnal primate (Jiang et
138 al., 2020; Mure et al., 2018). In this study we used the FRG[®]-triple KO mouse model that
139 exhibits a mutated Fumarylacetoacetate Hydrolase (*Fah*) and severe immunodeficiency
140 (*Rag2*^{-/-} and *Il2rg*^{-/-}) (Azuma et al., 2007). After transplantation with primary human
141 hepatocytes, the engrafted cells can repopulate the liver up to 80% due to positive selection
142 over rodent hepatocyte functionally impaired for FAH (Azuma et al., 2007). Further
143 improvement of this model was obtained through backcrossing FRG[®]-KO mice with the non-
144 obese diabetic (NOD) mice, which can more easily accept xenografts (Foquet et al., 2017;
145 Takenaka et al., 2007). The resulting model FRGN mice were engrafted with human
146 hepatocytes from a donor or murine hepatocyte from NOD mice to produce respectively liver-
147 humanized (Hu-FRGN[®], LHM) or control "murinized" mice (Mu-FRGN[®], LMM) (Minniti et al.,
148 2020) (**Figure 1A**). Circulating levels of human albumin (hAlb) in LHM were used to
149 corroborate the extent of human hepatocyte repopulation and were in average 6414±412
150 µg/ml in LHM while no hAlb could be detected in LMM (**Figure S1A**). Over the course of the
151 entire study, only mice with circulating levels of human albumin >3500 µg/mL (expecting to
152 correspond to human hepatocyte repopulation >70% (Ellis et al., 2013)) were used. An
153 additional functional readout of successful liver humanization was gathered through the
154 measure of triglycerides (TG) content in low density lipoprotein (LDL). While rodents
155 transport TG mainly in high density lipoproteins (HDL) (Ellis et al., 2013), TG in human serum
156 are typically enriched in liver-born LDL. Unlike LMM, LHM lipoprotein profile displayed

157 enrichment of TG in LDL, confirming the extent of liver humanization and in agreement with
158 previous observations (Minniti et al., 2020) (**Figure S1B**).

159 To decipher the impact of the transplantation of human hepatocytes on the rhythmic
160 physiology of the mouse liver, we analyzed liver rhythmic gene expression in LMM and LHM.
161 Both LMM and LHM mice, engrafted on the same week and exposed to the same nutritional
162 and pharmacologic treatment (see method) and housing conditions, were sacrificed every 4-
163 hours and liver tissue collected prior to RNA extraction and sequencing. Due to the high
164 depth RNA sequencing, we can discriminate between human and non-human RNA
165 orthologues within LHM liver samples, allowing independent normalization for the two
166 species before the analysis of differential rhythmicity of gene expression using our recently
167 developed *dryR* method (Weger et al., 2021) (**Figure 1B and S1C**). *dryR* assigns groups of
168 genes to various models of rhythmic behavior and species. For instance, genes assigned to
169 model 4 are rhythmic only in LMM while those in models 2, 3, 5, and 6 are arrhythmic in LMM
170 but displayed rhythm in LHM with similar or different species-specific rhythmic parameters
171 (**Figure 1B**).

172 The analysis reveals that the largest group (model 4) is composed of genes that lose
173 rhythmicity specifically in LHM animals, for both human and mouse transcripts (**Figure 1C,**
174 **1D, S1D, Table S1**). These genes show the classical biphasic pattern observed for rhythmic
175 genes regulated by systemic or feeding cues (**Figure 1D**) (Weger et al., 2021). These
176 rhythmic genes are mainly involved in protein synthesis and ribosome biogenesis,
177 suggesting an attenuated activation of the mechanistic target of rapamycin (mTOR) pathway
178 (**Table S2**). A comparison with the genes differentially expressed in the liver of *Raptor* or
179 *Tsc1* KO mice, the main positive and negative regulators of the TORC1 complex,
180 respectively (Bai et al., 2021), confirms that the genes differentially expressed in LHM are
181 indeed enriched in genes transcriptionally regulated by the mTOR pathway (**Figure S1E**).
182 Additional analysis of the phosphorylation of ribosomal protein S6 (RPS6, a bona fide
183 TORC1 target) confirms the absence of the expected rhythmic activation of this pathway in
184 the liver of LHM (Jouffe et al., 2013) (**Figure S1F**). The mTOR pathway being recognized as
185 a key sensor of systemic and nutritional signals (Saxton and Sabatini, 2017), this suggests
186 that the human hepatocytes are unable to respond to such signals when placed in a mouse
187 environment. Alternatively, the human hepatocytes can also respond to these signals in a
188 different manner that does not result in the rhythmic activation of the mTOR pathway. The
189 inappropriate response of human hepatocytes to mouse signals is also illustrated by the
190 blunted response to Growth Hormone (GH), an important regulator of the sex biased liver
191 function and metabolism (Al-Massadi et al., 2022; Lichanska and Waters, 2008). Indeed,
192 endogenous mouse GH is high while IGF-1 is low in LHM (**Figure S1G**). This shows that
193 human hepatocytes cannot secrete IGF-1 in response to GH and, in turn, the low level of

194 IGF-1 is not sufficient to exert its inhibitory action on GH secretion, resulting in constantly
195 high GH levels. As an additional evidence of the disruption of GH signaling, the sex biased
196 gene expression as well as the activation of the sex biased activation of the STAT5 pathway,
197 two recognized readouts of GH signaling (Weger et al., 2019; Zhang et al., 2012), are also
198 perturbed, with an increase of female biased signaling and a decrease of the male biased
199 signaling, likely as a result of the constantly high GH level (**Figure S1H**). The IGF-1 / mTOR
200 pathway being important for the synchronization of the circadian clock by systemic signals
201 (Crosby et al., 2019), this blunted response could contribute to the lack of entrainment of
202 human hepatocytes.

203 On the other hand, hundreds of genes mainly involved in angiogenesis and telomere
204 maintenance are only rhythmic in human hepatocytes (**model 2, Figure S1D**), suggesting
205 that these cells can express their own specific rhythmic physiological program different from
206 the one of mouse hepatocytes (**Figure S2A, S2B, Table S1, S2**). Of particular interest is
207 model 14 in which 110 genes are found to share similar phase advance in both human and
208 rodent cells in LHM compared to the liver of LMM (**Figure 2A, 2B, Table S1**). Surprisingly,
209 this group shows a clear enrichment to circadian clock related pathways (**Table S2**) and
210 includes most circadian clock and clock target genes (**Figure 2C**). This phase advance of
211 clock genes expression associated with a lower amplitude mirrors the presence of a
212 functional clock only in hepatocytes in a clock depleted animal (Koronowski et al., 2019),
213 suggesting that the human hepatocytes clock in a mouse liver operates like independent
214 oscillators not responding to synchronizing rhythmic systemic signals. To support this
215 hypothesis, we compared our results with the rhythmic genes present in the liver of wild-type,
216 *Bmal1* KO, and *Bmal1* KO with a specific rescue of *Bmal1* only in the liver (liver-RE), an
217 example of independent hepatocyte oscillator in a circadian clock depleted animal
218 (Koronowski et al., 2019). Interestingly, the genes that lost rhythmicity in the liver of LHM
219 (model 4) are specifically enriched in genes rhythmic only in WT animals (**Figure S2C**),
220 supporting the idea that these genes are indeed mainly regulated by systemic signals
221 originating from other organs in a circadian clock-dependent fashion, but independent of the
222 hepatocyte circadian clock. This confirms that the human hepatocytes cannot respond to
223 mouse synchronizing rhythmic systemic signals and operate largely independently from the
224 rest of the organism. The fact that the mouse hepatocytes in LHM mice show the same
225 circadian behavior suggests that the human hepatocytes can entrain the remaining mouse
226 cells in the liver of LHM.

227

228 **The muscle circadian clock of liver humanized mice is phase advanced**

229 To determine if this entrainment by human hepatocytes is specific to the mouse cells in the
230 liver, we performed a similar RNA-Seq analysis on the skeletal muscle (quadriceps) of LMM

231 and LHM (**Figure 3A**). While the biggest group of genes (model 4: 32%) shows similar
232 rhythms in LHM and LMM, a similar and important proportion of genes (model 2: 26% and
233 model 3: 28%, respectively) are only rhythmic in the muscle of LHM and LMM mice,
234 respectively, showing that human hepatocytes in LHM have a strong influence on the
235 rhythmicity of other tissues (**Figure S3A and Table S1**). The genes that lose rhythmicity in
236 LHM (model 3) are mainly involved in protein lipid and cholesterol metabolisms, showing the
237 impact of the human hepatocytes on the global physiology and metabolism of the animals
238 (**Figure S3B, S3C and Table S3**). Strikingly, the group of genes displaying different
239 circadian parameters (model 5: 13%) includes almost all the circadian clock genes and bona
240 fide clock target genes (**Figure 3B, 3C, S3A, Table S1 and S3**). While we did not find clear
241 effect on the amplitude, all these clock genes show an advanced phase of expression more
242 important than the one we found in the liver (**Figure 3D**). This result demonstrates that the
243 engraftment of human hepatocytes in mouse liver can surprisingly phase advance the
244 circadian clock of other peripheral tissues.

245

246 **Human hepatocytes advance the phase of circadian metabolism and behavior of liver** 247 **humanized mice**

248 Because feeding cues act as the main driver of the phase of peripheral clocks, disconnecting
249 them from the entrainment by the SCN (Damiola et al., 2000; Stokkan et al., 2001), we
250 hypothesized that the advanced phase of the muscle circadian clock could be a
251 consequence of a change of rhythmic metabolic and behavioral output driven by the
252 engrafted human hepatocytes. Therefore, we performed a comprehensive characterization of
253 the rhythmic physiology of LMM and LHM. Under a normal light/dark cycle, LHM strikingly
254 display an approximately 2hrs phase advance of locomotor activity, feeding behavior,
255 respiratory exchange ratio, and fat oxidation compared to LMM (**Figure 4A-H**). The
256 amplitude of the rhythmic locomotor activity and food intake is also decreased (**Figure S4A-**
257 **D**). Of note, LMM and LHM did not significantly differ in average cumulative food intake
258 (**Figure S4B**) and show only a slightly reduced body weight and body fat (**Figure S4E**),
259 suggesting that the change in entrainment properties did not result from metabolic
260 impairment. Altogether, this confirms that the phase advance observed in the muscle of LHM
261 is likely a consequence of the advanced feeding activity.

262 As described in the case of the familial advanced sleep-phase syndrome (FASP), this phase
263 advance observed in light/dark condition could be a consequence of a short circadian period
264 (Hirano et al., 2016; Jones et al., 1999; Xu et al., 2005; Xu et al., 2007). Accordingly, humans
265 with shorter circadian periods show an early chronotype (Brown et al., 2008; Duffy et al.,
266 2001). Thus, we determined the circadian period of the animals via the recording of their
267 circadian wheel-running activity in constant darkness (**Figure I**). Strikingly, LHM show a

268 significantly shorter period (**Figure 4J, 4K**), demonstrating feedback signals from human
269 hepatocytes to the central clock in the SCN. This suggests an unexpected and never
270 described impact of hepatocytes on the circadian function of the SCN.

271

272 **Engrafted human hepatocytes impact rhythmic gene expression in the hypothalamus**

273 To decipher how the engrafted human hepatocytes can extend their influence beyond the
274 liver and muscle to the brain centers involved in the control of metabolism and circadian
275 rhythms, we performed a time-resolved RNA-Seq experiment on the hypothalamic brain
276 punches of the Arcuate nucleus (ARC) and the SCN (**Figure 5A**). Relative enrichment of the
277 SCN-enriched gene *Aralkylamine N-Acetyltransferase (Aanat)* or ARC-enriched *Agouti*
278 *related peptide (Agrp)* confirms dissection accuracy (**Figure S5A**). The majority (58% and
279 53%, model 4) of the rhythmic genes keep their rhythmicity in the SCN and the ARC,
280 respectively, including the majority of circadian clock genes (**Figure S5B, S5C and Tables**
281 **S1**). However, the second largest group of genes representing 30% and 26% of the rhythmic
282 genes (model 3) loses rhythmicity in the SCN and the ARC of LHM, respectively, showing
283 that engraftment of human hepatocytes can unexpectedly impact the rhythmic gene
284 expression in the hypothalamus (**Figures 5B-E, S5B, S5C, and Tables S1**). These genes
285 that lose rhythmicity in the SCN and ARC of LHM are enriched for genes encoding proteins
286 involved in ions transport, critical for the function of neurons (Tables S4 and S5). In addition,
287 a small subset of 2% and 10% of rhythmic genes in the SCN and the ARC, respectively,
288 exhibits different circadian parameters between LMM and LHM (model 5, **Figure 5F-I**). In
289 contrast to liver and muscle, only a few circadian clock genes, including *Nr1d1* and *Dbp*, are
290 included in these groups, both showing a phase advance in LHM animals (**Figure S5D,**
291 **S5E**). Nevertheless, additional analysis shows that the genes in models 4 and 5 exhibit both
292 an enrichment for genes controlled by the circadian regulator CLOCK (Alhopuro et al., 2010).
293 This suggests that only a subset of circadian clock-controlled genes are phase advanced in
294 the hypothalamus, potentially because of conflicting light signals synchronizing the SCN
295 clock (Shigeyoshi et al., 1997; Xu et al., 2021) (**Figure S5F**). Altogether, these results show
296 that the human hepatocytes in LHM can impact the function of the hypothalamus, resulting in
297 a substantial loss of rhythmicity or a change of rhythmicity of gene expression in the SCN
298 and the ARC.

299

300 **Engraftment of human hepatocytes reveals the ability of hepatic signals to feedback** 301 **on the central pacemaker**

302 While the SCN is required for the coordination of feeding and drinking rhythms (Stephan and
303 Zucker, 1972; Van den Pol and Powley, 1979), a functional SCN counteracts and delays the
304 synchronization of mice to day feeding. Consequently, SCN-lesioned animals synchronized

305 their circadian peripheral clocks more rapidly to day feeding (Saini et al., 2013; Sinturel et al.,
306 2021). On the other hand, feeding rhythm is a very potent synchronizing signal for peripheral
307 tissues and can uncouple peripheral oscillators from the central clock (Damiola et al., 2000;
308 Stokkan et al., 2001). Because LHM show an advanced phase of physiology and a global
309 loss of rhythmic gene expression in the SCN, we speculate that the engraftment of human
310 hepatocyte can impact the capacity of the SCN to oppose the synchronization of animal
311 physiology to feeding during the light phase.

312 To test this hypothesis, LMM and LHM were subjected to a 5-days measurement of baseline
313 rhythmic physiology under *ad libitum* feeding, followed by a 7-days imposed feeding during
314 the light phase before returning to *ad libitum* feeding (**Figure 6A**). As described above, we
315 observed an advance in the phase of feeding and metabolic outputs at baseline conditions
316 (**Figure 6B, 6E, and S6A**) which were abolished during an imposed feeding regimen (**Figure**
317 **6C, 6F, S6A**). Strikingly, upon day 5 of return to *ad libitum* feeding, the advanced phase in
318 LHM reappeared (**Figure 6D, 6G, S6A**), showing that this phase advance is an intrinsic
319 property of the SCN of LHM. While around 40% of the locomotor activity of LMM shift to the
320 day, as expected as an adaptation to feeding during the light phase, they kept the circadian
321 component of their locomotor activity at night, even after 6 days of this regimen (**Figure 6H,**
322 **6I, 6L and S6B**). However, LHM loose this circadian component and shift rapidly most of
323 their daily locomotor activity to the light phase (**Figure 6H,6 I, 6L and S6B**). Of note, this lot
324 of LMM and LHM did no significantly differ in body weight and body fat (**Figure S6C**),
325 suggesting that the change in entrainment properties did not result from metabolic
326 impairment. More strikingly, while the drinking activity of LMM, which is imposed by the
327 central clock, is essentially restricted to the dark phase, it is shifted very rapidly to the light
328 phase in LHM. Thus, approximately 90% of drinking activity during the light phase was
329 observed already after 3 days (**Figure 6J, 6K, 6M and S6B**). This observation shows that
330 the implantation of human hepatocyte modifies the entrainment properties of the SCN of
331 LHM that becomes more sensitive to feeding cues and let them adapt more rapidly to
332 daytime feeding paradigm, reminiscent of the adaptation observed in SCN lesioned animals
333 (Saini et al., 2013).

334

335 **DISCUSSION**

336 The data presented here shows that the engraftment of human hepatocytes can impact on
337 the diurnal physiology and behavior of the grafted mice. Strikingly, the human hepatocytes
338 not only advance the phase of surrounding mouse liver cells, but also the phase of distant
339 muscle cells, likely through the change of global rhythmic physiology and behavior. Even
340 more surprising is the discovery that the human hepatocytes also influence the rhythmic
341 property of hypothalamic centers, probably by impacting the rhythmic gene expression in the
342 SCN and the ARC. These effects resulted in a shorter circadian period, a phase advanced
343 activity under a light-dark cycle, including the feeding rhythm, and a faster synchronization to
344 feeding cues. This suggests that a circadian oscillator in peripheral organs with different
345 circadian properties can feedback on brain centers to control circadian physiology and
346 behavior. While keeping central and peripheral clock in phase is clearly of paramount
347 importance, there are still some uncertainties as for the relative independence or total
348 subordination of peripheral oscillators versus the central clock. Uncertainties also exist on
349 how a peripheral organ rhythm can possibly modulate or even entrain the central clock.
350 Although the SCN is required to maintain synchrony between the peripheral organs (Izumo et
351 al., 2014; Sinturel et al., 2021; Yoo et al., 2004), the hepatocyte oscillator can work
352 autonomously (Koronowski et al., 2019) and the synchrony between the hepatocytes persists
353 in SCN-lesioned mice (Izumo et al., 2014; Sinturel et al., 2021). However, while the
354 hepatocyte clock has the ability to modulate the circadian physiology of other liver cells or
355 distant organs (Guan et al., 2020; Manella et al., 2021), no impact on the central circadian
356 clock has been reported. Hence, our data show for the first time that the hierarchy between
357 SCN and hepatocytes in the control of the circadian physiology can be challenged since
358 peripheral oscillators with different circadian rhythms and responses to systemic cues impact
359 the central oscillator.

360 Several mechanisms could be involved. The liver-brain axis could encompass rhythmic
361 secretion of liver-borne molecules acting centrally and/or peripherally together with nervous
362 pathway connecting these two organs. However, while several food-related hormones or
363 metabolites modulate the synchronization of peripheral clocks or feeding behavior in
364 response to nutrient signals, none of them have been shown to impact the central circadian
365 clock and modulate the circadian period of the animals (Bookout et al., 2013; Chen et al.,
366 2019; Landgraf et al., 2015). Of importance, the hepatocytes in LMM and LHM result from
367 the migration of injected hepatocytes in the spleen and transfer to the liver, followed with
368 positive selection of human hepatocytes and of healthy murine hepatocytes (Azuma et al.,
369 2007; Ellis et al., 2013; Minniti et al., 2020). In this procedure LMM and LHM retain the
370 architecture of liver-brain vagal connection. Hence, it is possible that the nervous connection
371 between the liver and the brain may have routed hepatic information able to modify the

372 central control of circadian physiology. In turn, modified central control will impede on
373 peripheral organs function through the hypothalamic-pituitary-adrenal axis and/or the
374 autonomic nervous system, resulting in peripheral tissue synchronization.

375 The misalignment of central and peripheral clocks due to shift work, jet lag, or desynchrony
376 between food and light signals (abnormal feeding pattern) has been implicated in various
377 diseases including sleep disorders, psychiatric disorders, and cardiometabolic disease,
378 including atherosclerosis, obesity, diabetes, and non-alcoholic fatty liver disease (Bishehsari
379 et al., 2016; Mokhlesi et al., 2019; Shan et al., 2018; Tan et al., 2018; Vetter et al., 2018).
380 Conversely, the metabolic syndrome is associated with disruption of circadian rhythms and
381 sleep (Lee et al., 2017; Zimmet et al., 2019). Mice exposed to a high fat diet exhibit an
382 alteration of their circadian clocks and feeding behavior (Kohsaka et al., 2007) and circadian
383 desynchrony impacting phase coherence between peripheral organs and communication
384 between peripheral and central clocks (Dyar et al., 2018). Moreover, high fat diet induces an
385 advance of phase of the liver circadian clock (Pendergast et al., 2013) and alters the
386 response of the central clock to light signals (Mendoza et al., 2008). Likely these changes
387 are rather a consequence of the metabolic syndrome caused by this regimen than the high
388 fat diet *per se*. Indeed, female or male mice from inbred lines that did not develop metabolic
389 syndrome did not display alteration of their circadian and feeding behavior (Buckley et al.,
390 2021; Palmisano et al., 2017). Interestingly, liver diseases in human were shown to alter the
391 function of the peripheral and central circadian clocks. Liver cirrhosis was associated with
392 sleep disturbances, delayed phase of diurnal skin temperature cycle (Bruyneel and Serste,
393 2018; Cordoba et al., 1998; Garrido et al., 2017), and shifted plasma melatonin and cortisol
394 profiles, two hormonal phase markers of the human SCN clock (Montagnese et al., 2010). In
395 conclusion, our study provides the first evidence that the implantation of hepatocytes with
396 independent self-sustained circadian clock with different responses to systemic cues can
397 advance behavioral and metabolic rhythms through action on hypothalamic centers.

398 While many studies in rodent have underscored the implication of hepatocyte circadian clock
399 on animal physiology, we describe here in mice with hepatocyte humanization the ability of
400 peripheral cells to feedback to the central clock to the extent of redefining the free-running
401 period and the phase of behavior and metabolism. Our study illustrates the benefit of
402 chimeric animals to decrypt the impact of peripheral tissues in the control of circadian
403 physiology. By taking advantages on the species-specific difference in cellular physiology,
404 LHM allow to probe hierarchical organization of the circadian system which would otherwise
405 be inaccessible in a homogenous rodent or human context. While our study does not provide
406 a simple molecular mechanism by which human hepatocyte are capable of entraining
407 tissues, our results force us to reconsider the importance of peripheral cues as Zeitgebers for
408 behavior and physiology. The reciprocal relationship between central and peripheral clocks

409 should be taken into account in future studies aimed at the dissection of circadian physiology
410 and metabolism. We believe that our results beg to reconsider the importance of the hepatic
411 signals as Zeitgebers. In that view, it is formally possible that the cardiometabolic diseases
412 associated with disrupted circadian rhythms could primarily originate in peripheral tissues
413 which in turn will promote desynchrony in the other tissues.
414

415 **EXPERIMENTAL PROCEDURES**

416

417 **Animal ethics**

418 All animal experiments were performed with approval of the Animal Care Committee of the
419 Université Paris Cité (CEB-25-2016; number: 004667.02) and the veterinary office of the
420 Canton of Vaud, Switzerland (authorization VD 3170). Chimeric animals were generated at
421 Yecuris Corporation (Tualatin, OR, USA) or Karolinska Institutet (Stockholm, Sweden). This
422 study was approved the animal care committee and complies with the Declaration of
423 Helsinki, and ethical approvals (2010/678-31/3 and S82-13) were obtained from local
424 authorities. All animal work was conducted according to approved Institutional Animal Care
425 and Use Committee (IACUC, Yecuris Corporation) protocol DN000024 and NIH OLAW
426 assurance #A4664-01. The protocols follow the NIH Guide for the Care and Use of
427 Laboratory Animals.

428

429 **Animals**

430 *Fah*^{-/-}, *Rag2*^{-/-}, *Il2rg*^{-/-} mice (FRG) were crossed with non-obese diabetic (NOD) mouse strain
431 to create FRGN mice (Yecuris, Tualatin, OR, USA), whose livers can be fully repopulated with
432 human or murine hepatocytes. Human liver tissue and hepatocytes were obtained through
433 the Liver Tissue Cell Distribution System, and the studies were exempted by IRB 0411142
434 since no human subjects were involved (University of Pittsburgh). Human and murine
435 hepatocytes were transplanted via splenic injections that allowed to repopulate the mouse
436 liver by maintaining on 2-(2-nitro-4- fluoromethylbenzoyl) cyclohexane -1,3-dione (CuRx™
437 Nitisinone (NTBC) in the drinking water, a medication that prevents hepatocyte death when
438 FAH deficiency is present. Engraftment is sustained over the life of the animal with an
439 appropriate regimen of Nitisinone (20-0026) and prophylactic treatment of Sulfamethoxazole
440 (SMX) / Trimethoprin (TMP) antibiotics (20-0037). Due to the impaired immune system of
441 these stains, they are susceptible to respiratory infections. Mice received prophylactic
442 antibiotic treatment cycles in order to minimize respiratory infections. Treatments with a
443 combination of SMX/TMP for 5 days twice a month greatly reduces the occurrence of
444 common respiratory infections as well as subsequent secondary infections. The final
445 concentration of SMX/TMP drinking water is 640µg/ml, 128 µg/ml (TMP) (CuRx™ SMX/TMP
446 Antibiotic Cat# 20-0037, Yecuris corporation) and 3% Dextrose (Sigma-Aldrich ref D9434).
447 The homozygous deletion of *fah* in FRGN mice which produces a fumarylacetoacetate
448 dehydrogenase deficiency that disrupts tyrosine metabolism, leading to buildup of
449 hepatotoxic metabolite, fumarylacetoacetate. With the administration of 2-(2-nitro-4-
450 fluoromethylbenzoyl) cyclohexane -1,3-dione (CuRx™ Nitisinone (NTBC) Cat# 20-0026), the
451 intracellular accumulation of fumarylacetoacetate is blocked and the mice live normal

452 immune deficient mouse lifespans. Mice are cycling on 8mg/l NTBC treatment with
453 SMX/TMP antibiotic and 3% of Dextrose for 3 days every 5 weeks. To maintain hydration of
454 the mice during the extended period off Nitisinone, it is best to use sterile drinking water that
455 contains 3% Dextrose. Because the dextrose provides an opportunistic environment for
456 bacterial growth, new containers of sterile dextrose water need to be prepared every week as
457 described previously (Azuma et al., 2007). Chimeric animals were generated at Yecuris
458 Corporation (Tualatin, OR, USA). Ten weeks old male mice FRGN® repopulated with human
459 hepatocytes (LHH, Hu-FRGN®) and FRGN® repopulated with murine hepatocytes (LMM,
460 Mu-FRGN®) (Cat#10-0013 and Cat#10-0009, YECURIS corporation, Oregon, USA). Mice
461 were maintained on on Pico Lab High Energy Mouse Diet 5LJ5 (LabDiet). Only mice with
462 human hepatocyte repopulation >70% (corresponding to circulating levels of human albumin
463 >3.5 mg/mL) were used in this study.

464 Detailed engraftment for experimental group is as follow: experimental group presented in
465 **Figure 1, 2, Figure S1A, C, D, E, H, Figure S2** is composed of 12 mice transplanted with
466 human female donor F1 HHF13022 (n=12, LHM-F1) and 12 mice transplanted with NOD
467 murine donor (n=12, LMM-F1). Experimental group presented **Figure 3, S1F, S3** is
468 composed of 5 mice transplanted with human male donor F1 HHM30017 and 10 mice
469 transplanted with human female donor HHF13022 (n=15, LHM-F1) and 12 mice transplanted
470 with NOD murine donor (n=12, LMM-F1). Experimental group presented **Figure 4 A-H, S1B,**
471 **S4** is composed of 6 mice transplanted with human female donor F1 HHF17006 plus 2 mice
472 transplanted with human male donor F1 (n=12, LHM-F1) and 12 mice transplanted with NOD
473 murine donor (n=12, LMM-F1), experimental group in Figure 4 I-K is composed of 5 mice
474 transplanted with human male donor F1 HHM30017 and 10 mice transplanted with human
475 female donor HHF13022 (n=15, LHM-F1) and 12 mice transplanted with NOD murine donor
476 (n=12, LMM-F1). Experimental group presented **Figure 5, 6, S1G, S5, S6** is composed of 12
477 mice transplanted with human female donor HHF13022 (n=12, LHM-F1) and 12 mice
478 transplanted with NOD murine donor (n=12, LMM-F1).

479

480 **Time-resolved tissue collection**

481 Except otherwise noticed, mice were kept under diurnal lighting conditions (12-hr light 12-hr
482 dark) with unrestricted access to food. Mice were sacrificed by at 4-hour intervals over 24
483 hours corresponding to ZT2, ZT6, ZT10, ZT14, ZT18 and ZT22 by decapitation and tissues
484 were dissected, snap-frozen in liquid nitrogen, and stored at -80°C until further processing.

485

486 **Serum samples**

487 Blood samples were collected in serum collection tubes and allowed to clot for 1 h at 4 °C on
488 ice. Tubes were centrifuged at 10,000 g for 5 min at 4 °C and serum was stored immediately

489 at -80 °C. During the data collection, serum samples were aliquoted and thawed no more
490 than twice.

491

492 **Human albumin measurement**

493 After 1,000 or 10,000x dilution with Tris-buffered saline, human albumin concentration was
494 measured with the Human Albumin ELISA Quantitation Kit (Bethyl E80-129) according to the
495 manufacturer's protocol, to monitor the progress of humanization of transplanted mice. 1000
496 µg/mL of circulating human albumin correlates with ~20% engraftment of human cells, 2000
497 µg/mL with ~40% and mice with 4000 µg/mL of human albumin showed approximately at
498 ~80% of human cells in the repopulated liver (Ellis et al., 2013).

499

500 **Plasma rodent growth hormone and IGF-1 measure**

501 Plasma rodent growth hormone (Ref.22-GHOMS-E01) and rodent IGF-1 (Ref. 22-IG1MS-
502 E01) content of each sample was measured in duplicate with a colorimetric assay provided
503 by ALPCO corporation. The absorbance from each sample was measured in duplicate using
504 a spectrophotometric microplate reader. The intra- and inter-assay coefficients of variation
505 for these kits were around 0.3-8%. Plasma samples were tested in duplicate within one
506 assay, and the results were expressed in terms of the standards supplied (ng/mL).

507

508 **Quantification of plasma lipoprotein lipids**

509 Lipoproteins were separated from 2.5 µL of individual plasma samples by size exclusion
510 chromatography (SEC), using a Superose 6 PC 3.2/300 column (GE Healthcare Bio-
511 Sciences AB, Uppsala, Sweden). Lipoproteins were eluted as a fraction appearing in the
512 exclusion volume of the sepharose column that contained VLDL, then LDL and last HDL. TG,
513 concentrations were calculated after integration of the individual chromatograms (Parini et
514 al., 2006; Pedrelli et al., 2014), generated by the enzymatic-colorimetric reaction with the
515 respective following kits, TG GPO-PAP (Roche Diagnostics, Mannheim, Germany).

516

517 **Indirect calorimetry metabolic analysis**

518 The indirect calorimetry system carries out preclinical non-invasive and fully automated
519 measurement of food and water intake, O₂ consumption, CO₂ production, respiratory quotient
520 (as an indicator of glycolic or oxidative metabolic status), whole energy expenditure together
521 with tridimensional (X, Y, Z) spontaneous activity and fine movement (Phenomaster, TSE
522 Systems GmbH) as described (Joly-Amado et al., 2012). Mice were monitored for whole
523 energy expenditure (EE) or Heat (H), oxygen consumption and carbon dioxide production,
524 respiratory exchange rate (RER = VCO₂/VO₂, where V is a volume), and locomotor activity
525 using calorimetric cages with bedding, food, and water (Labmaster, TSE Systems GmbH,

526 Bad Homburg, Germany). Ratio of gases was determined through an indirect open circuit
527 calorimeter. This system monitors O₂ and CO₂ concentration by volume at the inlet ports of
528 a tide cage through which a known flow of air is being ventilated (0.4 L/min) and compared
529 regularly to a reference empty cage. For optimum analysis, the flow rate was adjusted
530 according to the animal body weights to set the differential in the composition of the expired
531 gases between 0.4 and 0.9% (Labmaster, TSE Systems GmbH, Bad Homburg, Germany).
532 The flow was previously calibrated with O₂ and CO₂ mixture of known concentrations (Air
533 Liquide, S.A. France). Oxygen consumption, carbon dioxide production and energy
534 expenditure were recorded every 15 min for each animal during the entire experiment. Whole
535 energy expenditure was calculated using the Weir equation respiratory gas exchange
536 measurements. Food consumption was measured as the instrument combines a set of highly
537 sensitive feeding and drinking sensors for automated online measurements. Unless noted
538 otherwise mice had free access to food and water *ad libitum*. To allow measurement of every
539 ambulatory movement, each cage was embedded in a frame with an infrared light beam-
540 based activity monitoring system with online measurement at 100 Hz. The sensors for gases
541 and detection of movement operated efficiently in both light and dark phases, allowing
542 continuous recording. Mice were monitored for body weight and composition at the entry and
543 the exit of the experiment. Body mass composition (lean tissue mass, fat mass, free water
544 and total water content) was analyzed using an Echo Medical systems' EchoMRI (Whole
545 Body Composition Analyzers, EchoMRI, Houston, USA), according to manufacturer's
546 instructions. Briefly, mice were weighed before they were put in a mouse holder and inserted
547 in MRI analyser. Readings of body composition were given within 1 min. Data analysis was
548 performed on Excel XP using extracted raw value of VO₂ consumed, VCO₂ production
549 (express in mL/h), and energy expenditure (kcal/h). Subsequently, each value was
550 expressed by total body weight extracted from the EchoMRI analysis

551

552 **Imposed day feeding regimen**

553 Mice were individually housed for at least 2 weeks and body weight monitored daily. Mice
554 were then housed in cages allowing for measure of metabolic efficiency, food intake, water
555 intake, and locomotor activity (Phenomaster system described previously). After a 10 days
556 *ad libitum* feeding and baseline recording, mice were imposed a strict daylight feeding for 8
557 days (food available from ZT0 to ZT12) and return to normal regimen for 8 days.

558

559 **RNA extraction and sequencing**

560 Liver RNA were isolated using the RNeasy kit from QIAGEN according to the manufacturer's
561 recommendations. The integrity and the concentration of each RNA sample was assessed
562 using Agilent 2100 bioanalyzer. cDNA was prepared following the NEBNext® Ultra™ II

563 Directional RNA Library Prep Kit protocol (New England Biolabs). The libraries were
564 sequenced using paired-end 150 bp sequencing on a HiSeq 4000 System (Illumina). Muscle,
565 ARC, and SCN RNA were isolated using the RNAdvance Tissue kit from Beckman Coulter
566 according to the manufacturer's recommendations. The integrity and the concentration of
567 each RNA sample was assessed using Agilent Fragment Analyzer-96 and with Quant-It
568 Ribogreen from Life Technologies. Libraries were prepared following the TruSeq Stranded
569 mRNA Kit protocol from Illumina and sequenced using paired-end 126 bp sequencing on a
570 HiSeq 2500 System (Illumina).

571

572 **Analyse of rhythmicity**

573 STAR 2.4.0i (Dobin et al., 2013) was used to map RNA-seq reads onto a chimeric genome
574 consisting of the *Mus musculus* (GRCm38/mm10) and *Homo sapiens* (GRCh38/hg19)
575 reference sequences and to quantify the number of uniquely mapped reads per gene and
576 organism. For the liver data, human and mouse genes with on average more than 10 read
577 counts in LMM or LHM were retained. Human and mouse genes were matched using
578 mouse-human orthologs database from Ensembl. To assess differential rhythmicity and
579 mean differences of gene expression in RNA-Seq raw count data, we used the *dryR* method
580 based on a model selection framework with generalized linear models (Weger et al., 2021).
581 Genes with a BICW (likelihood to belong to the chosen rhythmic model) larger than 0.3 (liver)
582 or 0.5 (muscle, SCN, ARC) and a log₂ amplitude > 0.5 in at least one condition were used for
583 the functional and gene set enrichment analysis

584

585 **Functional and gene set enrichment analysis**

586 *GO analysis*

587 Gene set enrichment analysis was performed using enrichR (Kuleshov et al., 2016) with GO
588 Biological Process (2021) or GO Molecular Function (2021) databases. Terms with adjusted
589 p-value < 0.1, combined score > 50 and odds ratio > 6 were selected.

590 *mTOR targets*

591 Supplementary table with differential expression analysis was downloaded from (Bai et al.,
592 2021). Genes were considered as differentially expressed between wildtype and respectively
593 *Raptor* KO and *Tsc1* KO mice at ZT12, if absolute log₂ fold change was larger than 1 and p-
594 value smaller than 0.05. Statistical overrepresentation of those genes sets in genes
595 upregulated (log₂FC > 1, *dryR* chosen model mean 2) or downregulated (log₂FC < 1 and
596 *dryR* chosen model mean 2) in LHM v LMM liver was computed using a hypergeometric test.

597 *System-driven genes*

598 Supplementary table for rhythmicity analysis was download from (Koronowski et al., 2019).
599 For each category (WT, *Bmal1* KO, *Bmal1* Liver-RE), genes were defined as rhythmic if the

600 p-value was smaller than 0.05. Statistical overrepresentation of those gene sets in the
601 different rhythmic models of LHM and LMM (BICW > 0.5 and log2 amplitude > 0.5) was
602 assessed using a hypergeometric test.

603 *CLOCK*-target genes

604 The *CLOCK*-target gene set was retrieved from Alhopuro *et al.* (Alhopuro *et al.*, 2010). We
605 used hypergeometric testing to calculate overrepresentation of the geneset within the
606 statistical models identified by *dryR*. A threshold of BICW > 0.5 was applied to the data and
607 for the liver dataset an additional threshold on amplitude log2FC > 0.5.

608

609 **Sex-biased gene expression and activation of the STAT5 pathway**

610 To predict activities of transcription factors and sex biased genes, we employed ISMARA
611 (Balwiercz *et al.*, 2014) on the count data after variance stabilizing transformation (vst) (Love
612 *et al.*, 2014). Target genes for sex biased STAT5 targets and sex biased genes in mouse
613 liver were taken from Zhang *et al.* ((Zhang *et al.*, 2012)) and Weger *et al.* (Weger *et al.*,
614 2019), respectively.

615

616 **Detection of phospho-S6 and S6 ribosomal protein in mouse extracts**

617 Liver from LMM and LHM were resuspended into lysis buffer (PBS 150 mM NaCl, pH 7.5, 1
618 % Triton X-100, 2 mM NaF, 2 mM Na₃VO₄, protease inhibitors), sonicated (10 sec, 10 %
619 power) and lysed for 30 min at 4°C under agitation. The lysate was centrifuged for 20 min at
620 15,000 g (4°C) and the sample protein concentration was determined using Bradford's
621 method. 60 µg of each sample were separated by SDS-PAGE (4-12 %, Invitrogen) followed
622 by a transfer onto a nitrocellulose membrane (0.22 µm, GE Healthcare) for 1 h at 4°C. A
623 ponceau staining of the membrane was done to ensure equal protein loading. Membranes
624 were then blocked in 5 % bovine serum albumin (BSA) in TBST (Tris 20 mM, 150 mM NaCl,
625 pH 7.6, 0.1 % Tween-20) for 1 h and incubated overnight with phospho-S6 ribosomal protein
626 antibody (#2211, Cell Signaling) in 1 % BSA TBST at 4 °C. The next day, membranes were
627 washed 3 times with PBST prior to incubation with secondary antibody for 1 h at room
628 temperature. Membranes were then washed 3 more times and the signal was detected by
629 chemiluminescence using ECL Prime reagent (GE Healthcare) on an Amersham Imager 600
630 detection system (GE Healthcare, France). Membranes were later stripped using stripping
631 buffer (Tris 60 mM, pH 6.8, 2 % SDS, 100 mM β-mercaptoethanol) for 30 min at room
632 temperature, blocked in 5 % BSA TBST for 1 h and reprobbed with S6 ribosomal protein
633 antibody (#2317, Cell Signaling) using the same protocol as above. Signal analysis were
634 performed using ImageJ software taking as standard reference a fixed threshold of
635 fluorescence.

636

637 **Statistical analysis**

638 All statistical comparisons were performed with Prism 9 (GraphPad Software, La Jolla, CA,
639 USA). All the data were analyzed using either Student t-test (paired or unpaired) with equal
640 variances or One-way ANOVA or Two-way ANOVA. Cosinor parameters (acrophase, mean,
641 period, amplitude) results were analyzed by simple comparisons (unpaired t-test). In all
642 cases, significance threshold was automatically set at $p < 0.05$. ANOVA analyses were
643 followed by Bonferroni *post hoc* test for specific comparisons only when overall ANOVA
644 revealed a significant difference (at least $p < 0.05$).

645

646 **Data availability**

647 RNA-Seq raw files have been deposited in NCBI's Gene Expression Omnibus (GSE212079)

648 <https://www.ncbi.nlm.nih.gov/geo/query/acc.cgi?acc=GSE212079>

649

650

651

652 **ACKNOWLEDGMENTS**

653 We would also like to thank all of the consortium members of the EU-funded research project
654 HUMAN (Health and the Understanding of Metabolism, Aging and Nutrition,
655 <http://www.fp7human.eu/>) who have directly and indirectly contributed to the discussion of
656 the results. We thank Olja Kacanski for administrative support, Isabelle Le Parco, Ludovic
657 Maingault, Angélique Dauvin, Aurélie Djemat, Florianne Michel, Magguy Boa, and Daniel
658 Quintas for animals' care and Sabria Allithi for genotyping. We are grateful to Professor Ueli
659 Schibler for critical input in the manuscript. We acknowledge the technical platform
660 Functional and Physiological Exploration platform (FPE) of the Université de Paris (BFA -
661 UMR 8251), the animal core facility Buffon of the Université de Paris/Institut Jacques Monod,
662 and Aymen Kaabi (Nestlé Research) for animal experiments.

663

664 **AUTHOR CONTRIBUTIONS**

665 **Conceptualization:** A.S.D., M.Q., P.P., F.G., and S.L.; **Investigation:** A.S.D., M.Q., C.G.,
666 J.C., R.G.P.D., J.B., B.D.W., A.C., S.M., J.P., M.K., L.L.V., M.E.M., M.P., F.G.; **Formal Data**
667 **Analysis:** C.G., B.D.W., E.C.; **Resources:** J.B., E.M.W.; **Funding acquisition:** P.P., F.G.,
668 S.L.; **Supervision:** A.S.D., P.P., F.G., S.L.; **Writing – original draft:** F.G., S.L.; **Writing –**
669 **review & editing:** all authors.

670

671 **FUNDING**

672 This work has been financed by the HUMAN project (grant agreement no. 602757) within the
673 EU's Seventh Framework Program (FP7) for research, technological development, and
674 demonstration. F.G. receives support from the Institute for Molecular Bioscience, The
675 University of Queensland. M.Q. was supported by a postdoctoral contract from the Galician
676 Government type A (Xunta de Galicia ED481B2014/039-0) and type B (Xunta de Galicia
677 ED481B2018/004). M.Q. is currently funded by a research contract "Miguel Servet"
678 (CP21/00108) from the ISCIII and co-funded by the European Union. We acknowledge
679 funding supports from the Centre National la Recherche Scientifique (CNRS) and the
680 Université Paris Cité.

681

682 **CONFLICT OF INTEREST**

683 J.B. was formerly President and Chief Executive Officer of Yecuris Corporation. E.M.W. was
684 formerly Senior Scientist at Yecuris Corporation. C.G., B.D.W., A.P., S.M., J.P., M.K., and
685 F.G. are or were employees of Société des Produits Nestlé SA.

686

687 **REFERENCES**

- 688 Al-Massadi, O., Parini, P., Ferno, J., Luquet, S., and Quinones, M. (2022). Metabolic actions
689 of the growth hormone-insulin growth factor-1 axis and its interaction with the central nervous
690 system. *Rev Endocr Metab Disord*.
- 691 Alhopuro, P., Bjorklund, M., Sammalkorpi, H., Turunen, M., Tuupanen, S., Bistrom, M.,
692 Niittymaki, I., Lehtonen, H.J., Kivioja, T., Launonen, V., *et al.* (2010). Mutations in the
693 circadian gene CLOCK in colorectal cancer. *Mol Cancer Res* 8, 952-960.
- 694 Atger, F., Mauvoisin, D., Weger, B., Gobet, C., and Gachon, F. (2017). Regulation of
695 Mammalian Physiology by Interconnected Circadian and Feeding Rhythms. *Front Endocrinol*
696 (Lausanne) 8, 42.
- 697 Azuma, H., Paulk, N., Ranade, A., Dorrell, C., Al-Dhalimy, M., Ellis, E., Strom, S., Kay, M.A.,
698 Finegold, M., and Grompe, M. (2007). Robust expansion of human hepatocytes in Fah-/
699 /Rag2-/-/Il2rg-/- mice. *Nat Biotechnol* 25, 903-910.
- 700 Bai, X., Liao, Y., Sun, F., Xiao, X., and Fu, S. (2021). Diurnal regulation of oxidative
701 phosphorylation restricts hepatocyte proliferation and inflammation. *Cell Rep* 36, 109659.
- 702 Balwiercz, P.J., Pachkov, M., Arnold, P., Gruber, A.J., Zavolan, M., and van Nimwegen, E.
703 (2014). ISMARA: automated modeling of genomic signals as a democracy of regulatory
704 motifs. *Genome Res* 24, 869-884.
- 705 Barca-Mayo, O., Pons-Espinal, M., Follert, P., Armirotti, A., Berdondini, L., and De Pietri
706 Tonelli, D. (2017). Astrocyte deletion of Bmal1 alters daily locomotor activity and cognitive
707 functions via GABA signalling. *Nat Commun* 8, 14336.
- 708 Bishehsari, F., Levi, F., Turek, F.W., and Keshavarzian, A. (2016). Circadian Rhythms in
709 Gastrointestinal Health and Diseases. *Gastroenterology* 151, e1-5.
- 710 Bookout, A.L., de Groot, M.H., Owen, B.M., Lee, S., Gautron, L., Lawrence, H.L., Ding, X.,
711 Elmquist, J.K., Takahashi, J.S., Mangelsdorf, D.J., *et al.* (2013). FGF21 regulates
712 metabolism and circadian behavior by acting on the nervous system. *Nat Med* 19, 1147-
713 1152.
- 714 Brancaccio, M., Edwards, M.D., Patton, A.P., Smyllie, N.J., Chesham, J.E., Maywood, E.S.,
715 and Hastings, M.H. (2019). Cell-autonomous clock of astrocytes drives circadian behavior in
716 mammals. *Science* 363, 187-192.
- 717 Brown, S.A., Kunz, D., Dumas, A., Westermark, P.O., Vanselow, K., Tilmann-Wahnschaffe,
718 A., Herzel, H., and Kramer, A. (2008). Molecular insights into human daily behavior. *Proc*
719 *Natl Acad Sci U S A* 105, 1602-1607.
- 720 Bruyneel, M., and Serste, T. (2018). Sleep disturbances in patients with liver cirrhosis:
721 prevalence, impact, and management challenges. *Nat Sci Sleep* 10, 369-375.
- 722 Buckley, T.N., Omotola, O., Archer, L.A., Rostron, C.R., Kaminen, E.P., Llanora, J.D.,
723 Chalfant, J.M., Lei, F., Slade, E., and Pendergast, J.S. (2021). High-fat feeding disrupts daily
724 eating behavior rhythms in obesity-prone but not in obesity-resistant male inbred mouse
725 strains. *Am J Physiol Regul Integr Comp Physiol* 320, R619-R629.
- 726 Chen, S., Feng, M., Zhang, S., Dong, Z., Wang, Y., Zhang, W., and Liu, C. (2019). Angptl8
727 mediates food-driven resetting of hepatic circadian clock in mice. *Nat Commun* 10, 3518.
- 728 Cordoba, J., Cabrera, J., Lataif, L., Penev, P., Zee, P., and Blei, A.T. (1998). High
729 prevalence of sleep disturbance in cirrhosis. *Hepatology* 27, 339-345.
- 730 Crosby, P., Hamnett, R., Putker, M., Hoyle, N.P., Reed, M., Karam, C.J., Maywood, E.S.,
731 Stangherlin, A., Chesham, J.E., Hayter, E.A., *et al.* (2019). Insulin/IGF-1 Drives PERIOD
732 Synthesis to Entrain Circadian Rhythms with Feeding Time. *Cell* 177, 896-909 e820.
- 733 Damiola, F., Le Minh, N., Preitner, N., Kornmann, B., Fleury-Olela, F., and Schibler, U.
734 (2000). Restricted feeding uncouples circadian oscillators in peripheral tissues from the
735 central pacemaker in the suprachiasmatic nucleus. *Genes Dev* 14, 2950-2961.
- 736 Dobin, A., Davis, C.A., Schlesinger, F., Drenkow, J., Zaleski, C., Jha, S., Batut, P., Chaisson,
737 M., and Gingeras, T.R. (2013). STAR: ultrafast universal RNA-seq aligner. *Bioinformatics* 29,
738 15-21.

739 Duffy, J.F., Rimmer, D.W., and Czeisler, C.A. (2001). Association of intrinsic circadian period
740 with morningness-eveningness, usual wake time, and circadian phase. *Behav Neurosci* 115,
741 895-899.

742 Dyar, K.A., Lutter, D., Artati, A., Ceglia, N.J., Liu, Y., Armenta, D., Jastroch, M., Schneider,
743 S., de Mateo, S., Cervantes, M., *et al.* (2018). Atlas of Circadian Metabolism Reveals
744 System-wide Coordination and Communication between Clocks. *Cell* 174, 1571-1585 e1511.

745 Ellis, E.C., Naugler, W.E., Parini, P., Mork, L.M., Jorns, C., Zemack, H., Sandblom, A.L.,
746 Bjorkhem, I., Ericzon, B.G., Wilson, E.M., *et al.* (2013). Mice with chimeric livers are an
747 improved model for human lipoprotein metabolism. *PLoS One* 8, e78550.

748 Foquet, L., Wilson, E.M., Verhoye, L., Grompe, M., Leroux-Roels, G., Bial, J., and
749 Meuleman, P. (2017). Successful Engraftment of Human Hepatocytes in uPA-SCID and
750 FRG((R)) KO Mice. *Methods Mol Biol* 1506, 117-130.

751 Garrido, M., Saccardo, D., De Rui, M., Vettore, E., Verardo, A., Carraro, P., Di Vitofrancesco,
752 N., Mani, A.R., Angeli, P., Bolognesi, M., *et al.* (2017). Abnormalities in the 24-hour rhythm of
753 skin temperature in cirrhosis: Sleep-wake and general clinical implications. *Liver Int* 37,
754 1833-1842.

755 Greco, C.M., Koronowski, K.B., Smith, J.G., Shi, J., Kunderfranco, P., Carriero, R., Chen, S.,
756 Samad, M., Welz, P.S., Zinna, V.M., *et al.* (2021). Integration of feeding behavior by the liver
757 circadian clock reveals network dependency of metabolic rhythms. *Sci Adv* 7, eabi7828.

758 Guan, D., Xiong, Y., Trinh, T.M., Xiao, Y., Hu, W., Jiang, C., Dierickx, P., Jang, C.,
759 Rabinowitz, J.D., and Lazar, M.A. (2020). The hepatocyte clock and feeding control
760 chronophysiology of multiple liver cell types. *Science* 369, 1388-1394.

761 Hastings, M.H., Maywood, E.S., and Brancaccio, M. (2018). Generation of circadian rhythms
762 in the suprachiasmatic nucleus. *Nat Rev Neurosci* 19, 453-469.

763 Hirano, A., Shi, G., Jones, C.R., Lipzen, A., Pennacchio, L.A., Xu, Y., Hallows, W.C.,
764 McMahan, T., Yamazaki, M., Ptacek, L.J., *et al.* (2016). A Cryptochrome 2 mutation yields
765 advanced sleep phase in humans. *Elife* 5.

766 Izumo, M., Pejchal, M., Schook, A.C., Lange, R.P., Walisser, J.A., Sato, T.R., Wang, X.,
767 Bradfield, C.A., and Takahashi, J.S. (2014). Differential effects of light and feeding on
768 circadian organization of peripheral clocks in a forebrain *Bmal1* mutant. *Elife* 3.

769 Jiang, C., Li, P., Ruan, X., Ma, Y., Kawai, K., Suemizu, H., and Cao, H. (2020). Comparative
770 Transcriptomics Analyses in Livers of Mice, Humans, and Humanized Mice Define Human-
771 Specific Gene Networks. *Cells* 9.

772 Johnson, B.P., Walisser, J.A., Liu, Y., Shen, A.L., McDearmon, E.L., Moran, S.M., McIntosh,
773 B.E., Vollrath, A.L., Schook, A.C., Takahashi, J.S., *et al.* (2014). Hepatocyte circadian clock
774 controls acetaminophen bioactivation through NADPH-cytochrome P450 oxidoreductase.
775 *Proc Natl Acad Sci U S A* 111, 18757-18762.

776 Joly-Amado, A., Denis, R.G., Castel, J., Lacombe, A., Cansell, C., Rouch, C., Kassis, N.,
777 Dairou, J., Cani, P.D., Ventura-Clapier, R., *et al.* (2012). Hypothalamic AgRP-neurons control
778 peripheral substrate utilization and nutrient partitioning. *EMBO J* 31, 4276-4288.

779 Jones, C.R., Campbell, S.S., Zone, S.E., Cooper, F., DeSano, A., Murphy, P.J., Jones, B.,
780 Czajkowski, L., and Ptacek, L.J. (1999). Familial advanced sleep-phase syndrome: A short-
781 period circadian rhythm variant in humans. *Nat Med* 5, 1062-1065.

782 Jouffe, C., Cretenet, G., Symul, L., Martin, E., Atger, F., Naef, F., and Gachon, F. (2013).
783 The circadian clock coordinates ribosome biogenesis. *PLoS Biol* 11, e1001455.

784 Kohsaka, A., Laposky, A.D., Ramsey, K.M., Estrada, C., Joshu, C., Kobayashi, Y., Turek,
785 F.W., and Bass, J. (2007). High-fat diet disrupts behavioral and molecular circadian rhythms
786 in mice. *Cell Metab* 6, 414-421.

787 Kornmann, B., Schaad, O., Reinke, H., Saini, C., and Schibler, U. (2007). Regulation of
788 circadian gene expression in liver by systemic signals and hepatocyte oscillators. *Cold
789 Spring Harb Symp Quant Biol* 72, 319-330.

790 Koronowski, K.B., Kinouchi, K., Welz, P.S., Smith, J.G., Zinna, V.M., Shi, J., Samad, M.,
791 Chen, S., Magnan, C.N., Kinchen, J.M., *et al.* (2019). Defining the Independence of the Liver
792 Circadian Clock. *Cell* 177, 1448-1462 e1414.

793 Koronowski, K.B., and Sassone-Corsi, P. (2021). Communicating clocks shape circadian
794 homeostasis. *Science* 371.

795 Kuleshov, M.V., Jones, M.R., Rouillard, A.D., Fernandez, N.F., Duan, Q., Wang, Z., Koplev,
796 S., Jenkins, S.L., Jagodnik, K.M., Lachmann, A., *et al.* (2016). Enrichr: a comprehensive
797 gene set enrichment analysis web server 2016 update. *Nucleic Acids Res* 44, W90-97.

798 Lamia, K.A., Storch, K.F., and Weitz, C.J. (2008). Physiological significance of a peripheral
799 tissue circadian clock. *Proc Natl Acad Sci U S A* 105, 15172-15177.

800 Landgraf, D., Tsang, A.H., Leliavski, A., Koch, C.E., Barclay, J.L., Drucker, D.J., and Oster,
801 H. (2015). Oxyntomodulin regulates resetting of the liver circadian clock by food. *Elife* 4,
802 e06253.

803 Lee, S.W.H., Ng, K.Y., and Chin, W.K. (2017). The impact of sleep amount and sleep quality
804 on glycemic control in type 2 diabetes: A systematic review and meta-analysis. *Sleep Med*
805 *Rev* 31, 91-101.

806 Lichanska, A.M., and Waters, M.J. (2008). How growth hormone controls growth, obesity and
807 sexual dimorphism. *Trends Genet* 24, 41-47.

808 Love, M.I., Huber, W., and Anders, S. (2014). Moderated estimation of fold change and
809 dispersion for RNA-seq data with DESeq2. *Genome Biol* 15, 550.

810 Manella, G., Sabath, E., Aviram, R., Dandavate, V., Ezagouri, S., Golik, M., Adamovich, Y.,
811 and Asher, G. (2021). The liver-clock coordinates rhythmicity of peripheral tissues in
812 response to feeding. *Nat Metab* 3, 829-842.

813 Mendoza, J., Pevet, P., and Challet, E. (2008). High-fat feeding alters the clock
814 synchronization to light. *J Physiol* 586, 5901-5910.

815 Minniti, M.E., Pedrelli, M., Vedin, L.L., Delbes, A.S., Denis, R.G.P., Oorni, K., Sala, C.,
816 Pirazzini, C., Thiagarajan, D., Nurmi, H.J., *et al.* (2020). Insights From Liver-Humanized Mice
817 on Cholesterol Lipoprotein Metabolism and LXR-Agonist Pharmacodynamics in Humans.
818 *Hepatology* 72, 656-670.

819 Mokhlesi, B., Temple, K.A., Tjaden, A.H., Edelstein, S.L., Utzschneider, K.M., Nadeau, K.J.,
820 Hannon, T.S., Sam, S., Barengolts, E., Manchanda, S., *et al.* (2019). Association of Self-
821 Reported Sleep and Circadian Measures With Glycemia in Adults With Prediabetes or
822 Recently Diagnosed Untreated Type 2 Diabetes. *Diabetes Care* 42, 1326-1332.

823 Montagnese, S., Middleton, B., Mani, A.R., Skene, D.J., and Morgan, M.Y. (2010). On the
824 origin and the consequences of circadian abnormalities in patients with cirrhosis. *Am J*
825 *Gastroenterol* 105, 1773-1781.

826 Mure, L.S., Le, H.D., Benegiamo, G., Chang, M.W., Rios, L., Jillani, N., Ngotho, M., Kariuki,
827 T., Dkhissi-Benyahya, O., Cooper, H.M., *et al.* (2018). Diurnal transcriptome atlas of a
828 primate across major neural and peripheral tissues. *Science* 359.

829 Palmisano, B.T., Stafford, J.M., and Pendergast, J.S. (2017). High-Fat Feeding Does Not
830 Disrupt Daily Rhythms in Female Mice because of Protection by Ovarian Hormones. *Front*
831 *Endocrinol (Lausanne)* 8, 44.

832 Parini, P., Johansson, L., Broijersen, A., Angelin, B., and Rudling, M. (2006). Lipoprotein
833 profiles in plasma and interstitial fluid analyzed with an automated gel-filtration system. *Eur J*
834 *Clin Invest* 36, 98-104.

835 Patke, A., Young, M.W., and Axelrod, S. (2020). Molecular mechanisms and physiological
836 importance of circadian rhythms. *Nat Rev Mol Cell Biol* 21, 67-84.

837 Patton, A.P., Smyllie, N.J., Chesham, J.E., and Hastings, M.H. (2022). Astrocytes sustain
838 circadian oscillation and bidirectionally determine circadian period, but do not regulate
839 circadian phase in the suprachiasmatic nucleus. *J Neurosci*.

840 Pedrelli, M., Davoodpour, P., Degirolamo, C., Gomaraschi, M., Graham, M., Ossoli, A.,
841 Larsson, L., Calabresi, L., Gustafsson, J.A., Steffensen, K.R., *et al.* (2014). Hepatic ACAT2
842 knock down increases ABCA1 and modifies HDL metabolism in mice. *PLoS One* 9, e93552.

843 Pendergast, J.S., Braneky, K.L., Yang, W., Ellacott, K.L., Niswender, K.D., and Yamazaki,
844 S. (2013). High-fat diet acutely affects circadian organisation and eating behavior. *Eur J*
845 *Neurosci* 37, 1350-1356.

846 Ralph, M.R., Foster, R.G., Davis, F.C., and Menaker, M. (1990). Transplanted
847 suprachiasmatic nucleus determines circadian period. *Science* 247, 975-978.

848 Saini, C., Liani, A., Curie, T., Gos, P., Kreppel, F., Emmenegger, Y., Bonacina, L., Wolf, J.P.,
849 Poget, Y.A., Franken, P., *et al.* (2013). Real-time recording of circadian liver gene expression
850 in freely moving mice reveals the phase-setting behavior of hepatocyte clocks. *Genes Dev*
851 *27*, 1526-1536.

852 Saxton, R.A., and Sabatini, D.M. (2017). mTOR Signaling in Growth, Metabolism, and
853 Disease. *Cell* *168*, 960-976.

854 Shan, Z., Li, Y., Zong, G., Guo, Y., Li, J., Manson, J.E., Hu, F.B., Willett, W.C.,
855 Schernhammer, E.S., and Bhupathiraju, S.N. (2018). Rotating night shift work and
856 adherence to unhealthy lifestyle in predicting risk of type 2 diabetes: results from two large
857 US cohorts of female nurses. *BMJ* *363*, k4641.

858 Shigeyoshi, Y., Taguchi, K., Yamamoto, S., Takekida, S., Yan, L., Tei, H., Moriya, T.,
859 Shibata, S., Loros, J.J., Dunlap, J.C., *et al.* (1997). Light-induced resetting of a mammalian
860 circadian clock is associated with rapid induction of the mPer1 transcript. *Cell* *91*, 1043-1053.

861 Sinturel, F., Gos, P., Petrenko, V., Hagedorn, C., Kreppel, F., Storch, K.F., Knutti, D., Liani,
862 A., Weitz, C., Emmenegger, Y., *et al.* (2021). Circadian hepatocyte clocks keep synchrony in
863 the absence of a master pacemaker in the suprachiasmatic nucleus or other extrahepatic
864 clocks. *Genes Dev* *35*, 329-334.

865 Stephan, F.K., and Zucker, I. (1972). Circadian rhythms in drinking behavior and locomotor
866 activity of rats are eliminated by hypothalamic lesions. *Proc Natl Acad Sci U S A* *69*, 1583-
867 1586.

868 Stokkan, K.A., Yamazaki, S., Tei, H., Sakaki, Y., and Menaker, M. (2001). Entrainment of the
869 circadian clock in the liver by feeding. *Science* *291*, 490-493.

870 Takenaka, K., Prasolava, T.K., Wang, J.C., Mortin-Toth, S.M., Khalouei, S., Gan, O.I., Dick,
871 J.E., and Danska, J.S. (2007). Polymorphism in *Sirpa* modulates engraftment of human
872 hematopoietic stem cells. *Nat Immunol* *8*, 1313-1323.

873 Tan, X., Chapman, C.D., Cedernaes, J., and Benedict, C. (2018). Association between long
874 sleep duration and increased risk of obesity and type 2 diabetes: A review of possible
875 mechanisms. *Sleep Med Rev* *40*, 127-134.

876 Tso, C.F., Simon, T., Greenlaw, A.C., Puri, T., Mieda, M., and Herzog, E.D. (2017).
877 Astrocytes Regulate Daily Rhythms in the Suprachiasmatic Nucleus and Behavior. *Curr Biol*
878 *27*, 1055-1061.

879 Van den Pol, A.N., and Powley, T. (1979). A fine-grained anatomical analysis of the role of
880 the rat suprachiasmatic nucleus in circadian rhythms of feeding and drinking. *Brain Res* *160*,
881 307-326.

882 Vetter, C., Dashti, H.S., Lane, J.M., Anderson, S.G., Schernhammer, E.S., Rutter, M.K.,
883 Saxena, R., and Scheer, F. (2018). Night Shift Work, Genetic Risk, and Type 2 Diabetes in
884 the UK Biobank. *Diabetes Care* *41*, 762-769.

885 Weger, B.D., Gobet, C., David, F.P.A., Atger, F., Martin, E., Phillips, N.E., Charpagne, A.,
886 Weger, M., Naef, F., and Gachon, F. (2021). Systematic analysis of differential rhythmic liver
887 gene expression mediated by the circadian clock and feeding rhythms. *Proc Natl Acad Sci U*
888 *S A* *118*.

889 Weger, B.D., Gobet, C., Yeung, J., Martin, E., Jimenez, S., Betrisey, B., Foata, F., Berger,
890 B., Balvay, A., Foussier, A., *et al.* (2019). The Mouse Microbiome Is Required for Sex-
891 Specific Diurnal Rhythms of Gene Expression and Metabolism. *Cell Metab* *29*, 362-382
892 e368.

893 Xu, P., Berto, S., Kulkarni, A., Jeong, B., Joseph, C., Cox, K.H., Greenberg, M.E., Kim, T.K.,
894 Konopka, G., and Takahashi, J.S. (2021). NPAS4 regulates the transcriptional response of
895 the suprachiasmatic nucleus to light and circadian behavior. *Neuron* *109*, 3268-3282 e3266.

896 Xu, Y., Padiath, Q.S., Shapiro, R.E., Jones, C.R., Wu, S.C., Saigoh, N., Saigoh, K., Ptacek,
897 L.J., and Fu, Y.H. (2005). Functional consequences of a CK1delta mutation causing familial
898 advanced sleep phase syndrome. *Nature* *434*, 640-644.

899 Xu, Y., Toh, K.L., Jones, C.R., Shin, J.Y., Fu, Y.H., and Ptacek, L.J. (2007). Modeling of a
900 human circadian mutation yields insights into clock regulation by PER2. *Cell* *128*, 59-70.

901 Yoo, S.H., Yamazaki, S., Lowrey, P.L., Shimomura, K., Ko, C.H., Buhr, E.D., Siepkka, S.M.,
902 Hong, H.K., Oh, W.J., Yoo, O.J., *et al.* (2004). PERIOD2::LUCIFERASE real-time reporting

903 of circadian dynamics reveals persistent circadian oscillations in mouse peripheral tissues.
904 Proc Natl Acad Sci U S A *101*, 5339-5346.
905 Zhang, Y., Laz, E.V., and Waxman, D.J. (2012). Dynamic, sex-differential STAT5 and BCL6
906 binding to sex-biased, growth hormone-regulated genes in adult mouse liver. Mol Cell Biol
907 *32*, 880-896.
908 Zimmet, P., Alberti, K., Stern, N., Bilu, C., El-Osta, A., Einat, H., and Kronfeld-Schor, N.
909 (2019). The Circadian Syndrome: is the Metabolic Syndrome and much more! J Intern Med
910 *286*, 181-191.

911

912

913

914 **FIGURE LEGENDS**

915 **Figure 1. Engraftment of human hepatocyte impacts liver rhythmic gene expression**

916 **A).** Model for humanized *Fah*^{-/-}, *Rag2*^{-/-}, *Il2rg*^{-/-} (FRG®-KO) that can be repopulated with
917 primary human (red) or murine (black) hepatocytes to produce liver humanized (LHM) or
918 “murinized” (LMM) mice.

919 **B)** Experimental design for liver tissue collection prior to RNA extraction, sequencing and
920 analyzing according to gene expression rhythmic properties. Alteration of rhythmic gene
921 expression of murine transcript in the liver of LMM (black, Mu RNA) and both murine (red,
922 Mu-RNA) and human transcript (red Hu-RNA) in the liver of LHM mice is assessed by model
923 selection (model 1–15): black line, stable transcription; black wave, rhythmic transcription;
924 red or green waves, rhythmic profiles with different rhythmic parameters (i.e., phase and/or
925 amplitude).

926 **C)** Heat maps of normalized rhythmic mRNA levels (BICW > 0.3, log2 amplitude > 0.5) in the
927 liver of LMM (black) and LHM (red) murine and human transcript (red) in the liver of LMM
928 and LHM. RNA presented here belonged to model 4 where genes were rhythmic only in
929 LMM

930 **D)** Radial plot of the distribution peak phase of expression for genes rhythmic only in the liver
931 of LMM (model 4).

932

933 **Figure 2. Engraftment of human hepatocyte impacts the phase of the liver circadian**
934 **clock**

935 **A)** Heat maps of normalized rhythmic mRNA levels (BICW > 0.3, log2 amplitude > 0.5) in the
936 liver of LMM (black) and LHM (red) murine and human transcript (red) in the liver of LMM
937 and LHM. Genes presented here belonged to model 14 where both LHM-Mu & LHM-Hu
938 orthologue transcripts share the same phase which is different from LMM.

939 **B)** Radial plot distribution of the peak phase of expression for rhythmic genes in the liver of
940 LMM and murine and human orthologue in the liver of LHM from model 14.

941 **C)** Rhythmic expression of circadian clock genes for murine (black, LMM) and murine (LHM-
942 Mu) and human (LHM-Hu) RNA orthologue in the humanized liver. Data are expressed as
943 mean +/- SEM (n=12 mice per groups, 2 points per replicates). For statistical details, see
944 Table S1.

945

946 **Figure 3. The muscle circadian clock of liver humanized mice is phase advanced**

947 **A)** Experimental design for muscle tissue collection prior to RNA extraction, sequencing and
948 analyzing according to rhythmic properties, alteration of rhythmic gene expression of murine
949 transcript in the muscle of LMM (black) and LHM (red) assessed by model selection (model

950 1–5): black line, stable transcription; black wave, rhythmic transcription; red wave, rhythmic
951 profiles with different rhythmic parameters (i.e., phase and/or amplitude).

952 **B)** Heat maps of normalized rhythmic muscle mRNA levels (BICW > 0.5, log2 amplitude >
953 0.5) in LMM (black) and LHM (red) from model 5 where LMM and LHM muscle transcript are
954 rhythmic but with different phase.

955 **C)** Radial plot distribution of the peak phase of expression for rhythmic genes in the liver of
956 LMM and murine and human orthologue in the liver of LHM from model 5.

957 **D)** Rhythmic expression of circadian clock genes in the muscle of LMM and LHM. Data are
958 expressed as mean +/- SEM (n=11-12 animals per groups). For statistical details, see table
959 S1.

960

961 **Figure 4. Human hepatocytes advance the phase of circadian metabolism and**
962 **behavior of liver humanized mice**

963 **A-D)** Metabolic evaluation of LMM and LHM represented as 3-days average spontaneous
964 locomotor activity (**A**), food intake (**B**, kcal/hr/kg of lean body weight), respiratory exchange
965 ratio (RER, **C**), and fat oxidation (**D**). Insert are showing magnification of the ZT8-12 time
966 window.

967 **E-H)** Cosinor analysis of rhythmic parameters acrophase (c) for locomotor activity (**E**), food
968 intake (**F**), RER (**G**), and fat oxidation (**H**).

969 **I)** Experimental design for the determination the circadian period of LMM and LHM via the
970 recording of the circadian running wheel activity in constant darkness.

971 **J)** Representative actogram and circadian period in LMM and LHM.

972 **K)** Circadian period of locomotor activity in LHM and LMM (n=12 and 15 for LMM and LHM,
973 respectively).

974 Codes for statistical values: * P<0.05, ** P<0.01, *** P<0.0001.

975

976 **Figure 5. Engrafted human hepatocytes impact rhythmic gene expression in the**
977 **hypothalamus**

978 **A)** Experimental design for SCN and ARC samples collection prior to RNA extraction,
979 sequencing and analyzing according to rhythmic properties, alteration of rhythmic gene
980 expression of murine transcript in the liver of LMM (black) and LHM (red) assessed by model
981 selection (model 1–5): black line, stable transcription; black wave, rhythmic transcription; red
982 wave, rhythmic profiles with different rhythmic parameters (i.e., phase and/or amplitude).

983 **B-E)** Heat maps of normalized rhythmic mRNA levels (BICW > 0.5, log2 amplitude > 0.5) and
984 radial plot of the distribution of the peak phase of expression of the cycling genes and in the
985 SCN (**B, C**) and ARC (**D, E**) in LMM (black) and LHM (red) from genes that lost rhythmicity in
986 LHM (model 3).

987 **F-I)** Heat maps of normalized rhythmic mRNA levels (BICW > 0.5, log2 amplitude > 0.5) and
988 radial plot of the distribution of the peak phase of expression of the cycling genes and in the
989 SCN (**F, G**) and ARC (**H, I**) in LMM (black) and LHM (red) from genes that show altered
990 rhythmic parameters in LHM (model 5).

991

992 **Figure 6. Engraftment of human hepatocytes reveals the ability of hepatic signals to**
993 **feedback on the central pacemaker**

994 **A)** Experimental design for the imposed feeding regimen during the light phase.

995 **B-G)** 2-days average analysis of rhythmic food intake (**B-D**) and RER (**E-F**) during the
996 baseline period (**B, E**), imposed daylight feeding (**C, F**), or day 5 after return to *ad libitum*
997 feeding (**D, G**) in LMM (black) and LHM (red) (n=6 per groups).

998 **H-K)** Representative of average distribution and non-linear cosinor fitting of baseline day 4
999 (**H, J**) and after 1 and 6 days of imposed light phase feeding rhythm (**I, K**) for locomotor
1000 activity (**H, I**) and water consumption (**J, K**).

1001 **L, M)** Evolution locomotor activity (**L**) and water intake (**M**) during the light-phase (LP) after
1002 transition from baseline (blue) to imposed feeding during the light phase (orange) as a
1003 percentage of baseline value. Data are expressed as mean +/- SEM (n=6 animal per
1004 condition). * P<0.05, ** P<0.01, *** P<0.0001.

1005

1006 **SUPPLEMENTARY FIGURE LEGENDS**

1007 **Figure S1. Characterization of the humanized mouse model and its impact on liver**
1008 **gene expression**

1009 **A)** Plasma level for human albumin in LHM mice 2 months after primary hepatocyte
1010 engraftment and prior to sacrifice at different ZT time. Human albumin is non-detectable in
1011 LMM.

1012 **B)** Plasma triglyceride (TG) Lipoprotein profile and in LMM and LHM.

1013 **C)** Proportion of human (red) and murine (black) reads counts in the liver of humanized
1014 (LHM) or “murinized” (LMM) model.

1015 **D)** Number of genes in all models of rhythmic gene expression (Figure 1B) in the liver of
1016 LMM and LHM (BICW > 0.3, log2 amplitude > 0.5).

1017 **E)** Enrichment of up- and down-regulated genes in the liver of LMM and LHM for genes up-
1018 and down-regulated in the liver of mice KO for the negative (*Tsc1* KO) or positive (*Raptor*
1019 KO) regulators of mTOR (see methods).

1020 **F)** Western blot analysis of Phospho-S6 Ribosomal Protein (Ser240/244) and total S6
1021 Ribosomal Protein and non-linear cosinor fitting of P-RPS6 signal normalized by ponceau
1022 signal. Analysis of rhythmicity done with *dryR* (BICW = 0.572 for rhythmicity only in LMM).

1023 **G)** Circulating murine growth hormone (GH) and Insulin-like growth factor-1 (IGF-1) in LMM
1024 and LHM. Data are expressed as mean +/- SEM (n=9-11 animals for each condition). ***
1025 P<0.0001.

1026 **H)** Top. Female- (left) and male(right)-biased gene expression from control and humanized
1027 mouse livers at indicated Zeitgeber Time (color). Bottom. The predicted activity of sex
1028 dependent (female (♀, left) and male (♂, right) target genes of STAT5 in the mouse liver. P
1029 values were determined by a two-way ANOVA (time, condition), P value for condition is
1030 reported (n = 12 mice per condition).

1031

1032 **Figure S2. Impact of the engrafted human hepatocytes on liver rhythmic gene**
1033 **expression**

1034 **A, B)** Heat maps (**A**) and radial plot of the distribution of the peak phase (**B**) of normalized
1035 rhythmic mRNA levels (BICW > 0.5, log2 amplitude > 0.5) in the liver of LMM (black) and
1036 LHM (red). Genes are assigned to model 2 in which only human genes are rhythmic in LHM
1037 animals while non-rhythmic in LMM.

1038 **C)** Enrichment of the rhythmic genes (-log10 p-value, hypergeometric test, see method) in
1039 the liver of LMM and LHM ranked in the 15 models of rhythmicity for genes rhythmic in all
1040 combinations of WT, *Bmal1* KO (KO), and hepatocyte specific *Bmal1* rescue in *Bmal1* KO
1041 animals (liver-RE). While genes directly regulated by BMAL1 (rhythmic in WT and liver-KO)
1042 are enriched in models 4 (rhythmic only in LMM), 11 (same rhythm in LMM and mouse and

1043 human transcripts in LMM), and 14 (rhythmic in all conditions but different phase in LMM),
1044 rhythmic genes dependent on systemic cues regulated by BMAL1 (rhythmic only in WT) are
1045 enriched only in model 4, showing that the rhythm of many of these genes depends on
1046 systemic signals regulated by the circadian clock in non-liver tissues.

1047

1048 **Figure S3. The muscle circadian clock of liver humanized mice is phase advanced**

1049 **A)** Number of genes in all models of rhythmic gene expression (Figure 3A) in the muscle of
1050 LMM and LHM (BICW > 0.5, log₂ amplitude > 0.5).

1051 **B, C)** Heat maps (**B**) and radial plot of the distribution of the peak phase (**C**) of normalized
1052 rhythmic mRNA levels (BICW > 0.5, log₂ amplitude > 0.5) in the muscle of LMM (black) and
1053 LHM (red). Genes are assigned to model 3 in which mRNA are only rhythmic in LMM.

1054

1055 **Figure S4. Human hepatocytes advance the phase of circadian metabolism and**
1056 **behavior of liver humanized mice**

1057 **A-D)** Cosinor analysis of the rhythmic parameters mean level (a) and amplitude (b) for
1058 locomotor activity (**A**), food intake (**B**), RER (**C**), and fat oxidation (**D**). Data are expressed as
1059 mean +/- SEM (n=6 animals per condition). * P<0.05, ** P<0.01

1060 **E)** Averaged values for body weight, lean body mass, and fat mass in LMM (black) and LHM
1061 (red) at the beginning of the experiment. Data are expressed as mean +/- SEM (n=6 per
1062 condition). P values were determined by a one-way ANOVA. * P<0.05, ** P<0.01.

1063

1064 **Figure S5. Engrafted human hepatocytes impact rhythmic gene expression in the**
1065 **hypothalamus A)** Expression level of the ARC-enriched *Agouti related transcript (Agrp)* and
1066 the SCN-enriched *Aralkylamine N-Acetyltransferase (Aanat)* in the dissected ARC and SCN
1067 of LMM (black) and LHM (red). **

1068 **B, C)** Number of genes in all models of rhythmic gene expression (Figure 5A) in the SCN (**B**)
1069 and ARC (**C**) of LMM and LHM.

1070 **D, E)** Rhythmic expression of the circadian clock regulated genes *Nr1d1* (D) and *Dbp* (E) in
1071 the SCN and ARC, respectively, of LMM and LHM.

1072 **F)** Enrichment of the rhythmic genes in the SCN and ARC of LMM and LHM ranked in the 5
1073 models of rhythmicity for genes bound by CLOCK in ChIP-Seq experiment (see Method).

1074

1075 **Figure S6. Engraftment of human hepatocytes reveals the ability of hepatic signals to**
1076 **feedback on the central pacemaker**

1077 **A)** Cosinor analysis of the acrophase (c) for RER during baseline (left), imposed feeding
1078 during the light phase (middle) and after return to *ad libitum* feeding (right). Data are
1079 expressed as mean +/- SEM (n=6 per condition). ** P<0.01, *** P<0.0001.

1080 **B)** Averaged values and kinetics of water intake in LMM mice (black upper panel) and LHM
1081 mice (red, lower panel) during baselines (blue, left Y axis) and imposed feeding rhythm
1082 (orange, right Y axis).
1083 **C)** Averaged values for body weight, lean body mass and fat mass in LMM (black) and LHM
1084 (red) at the beginning of the experiment. Data are expressed as mean +/- SEM (n=6 per
1085 condition). P values were determined by a one-way ANOVA.
1086

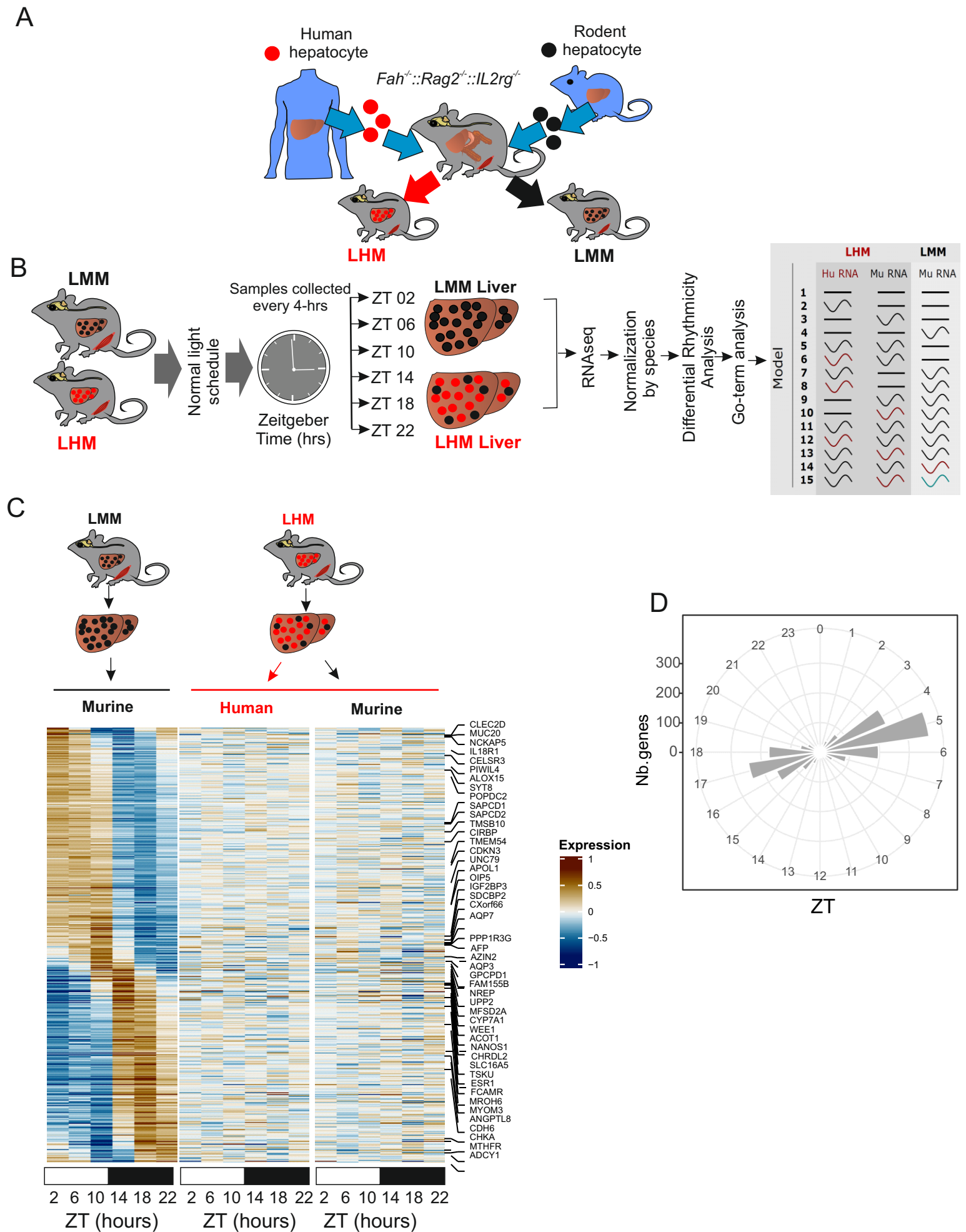


Figure 1

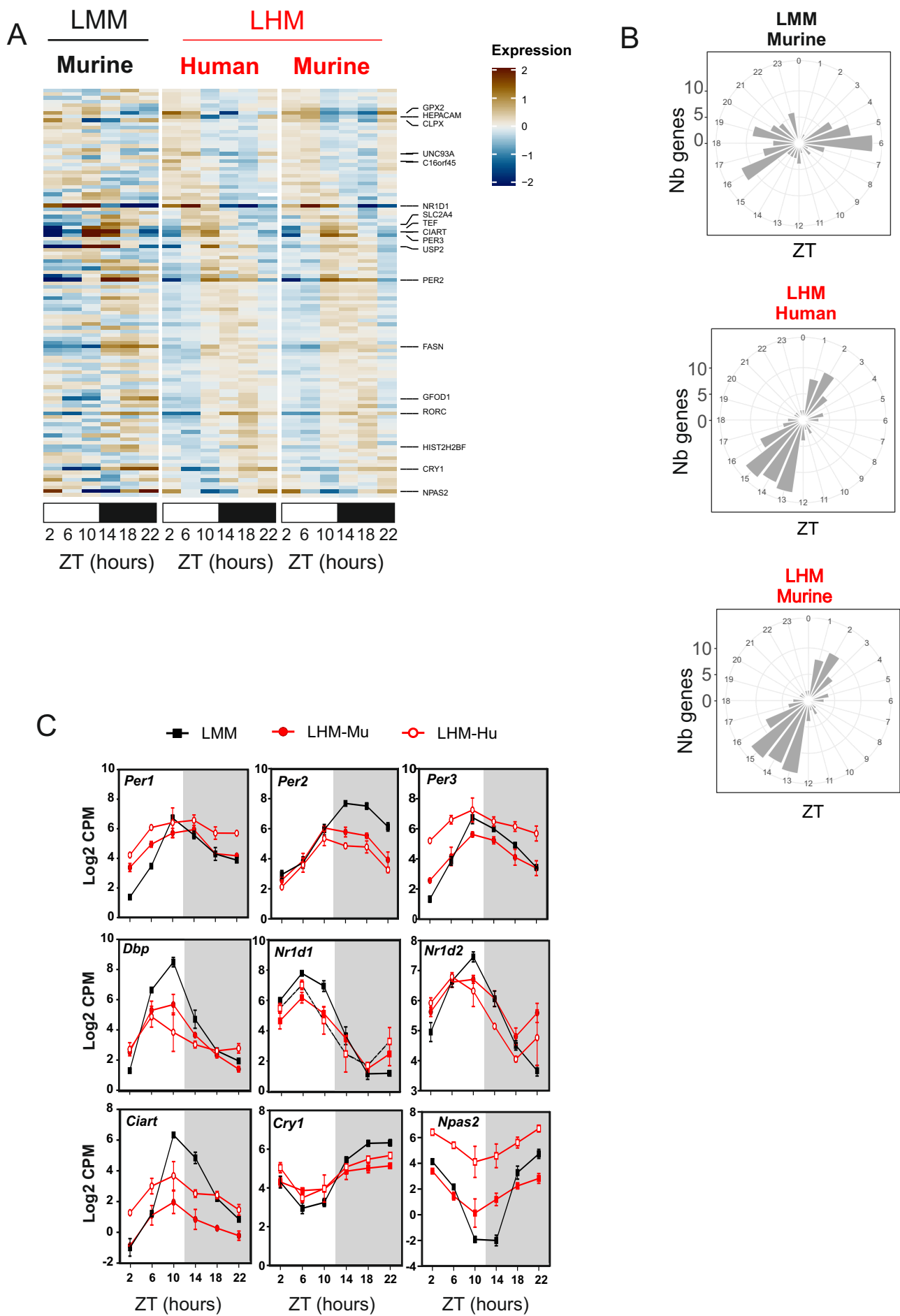


Figure 2

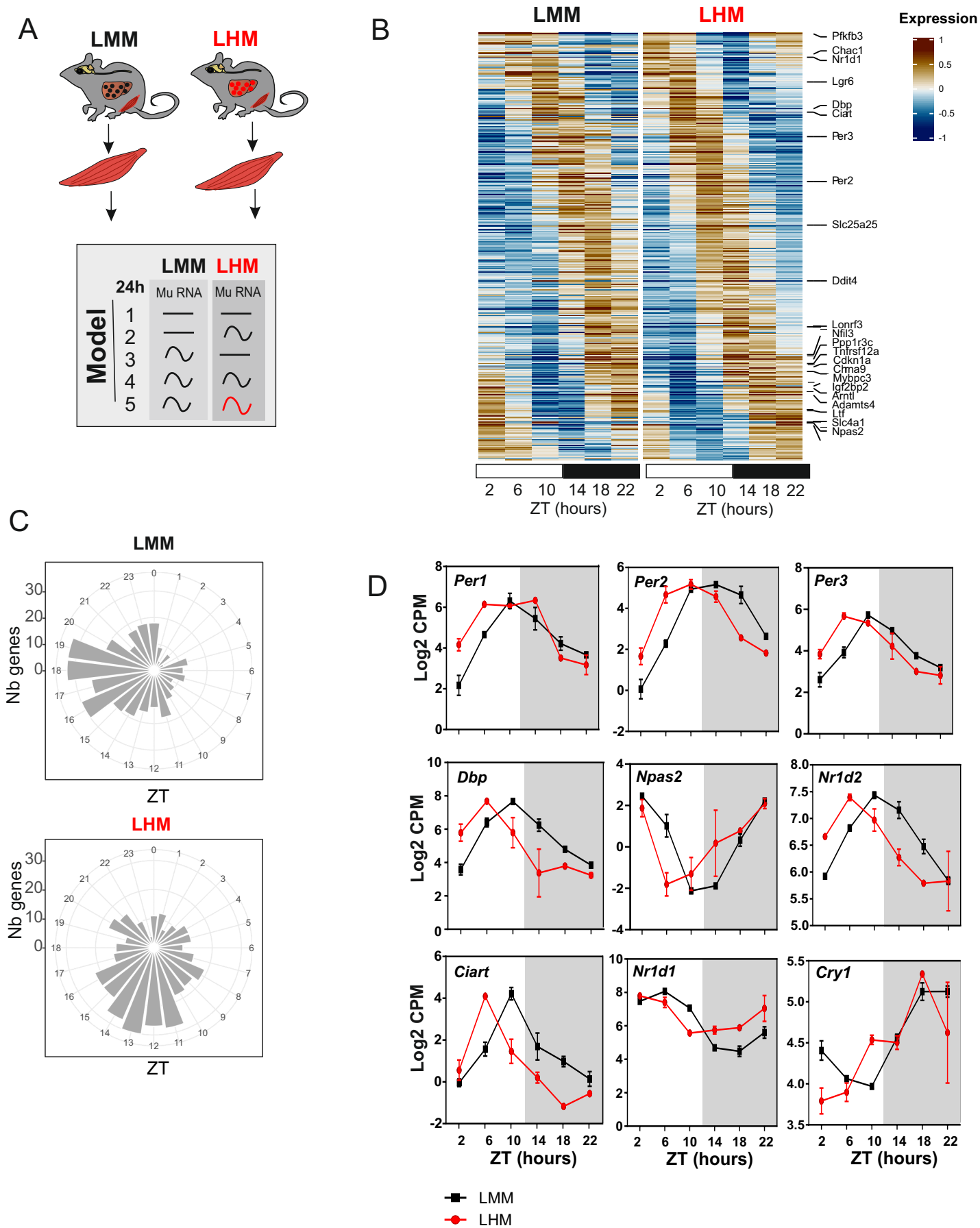


Figure 3

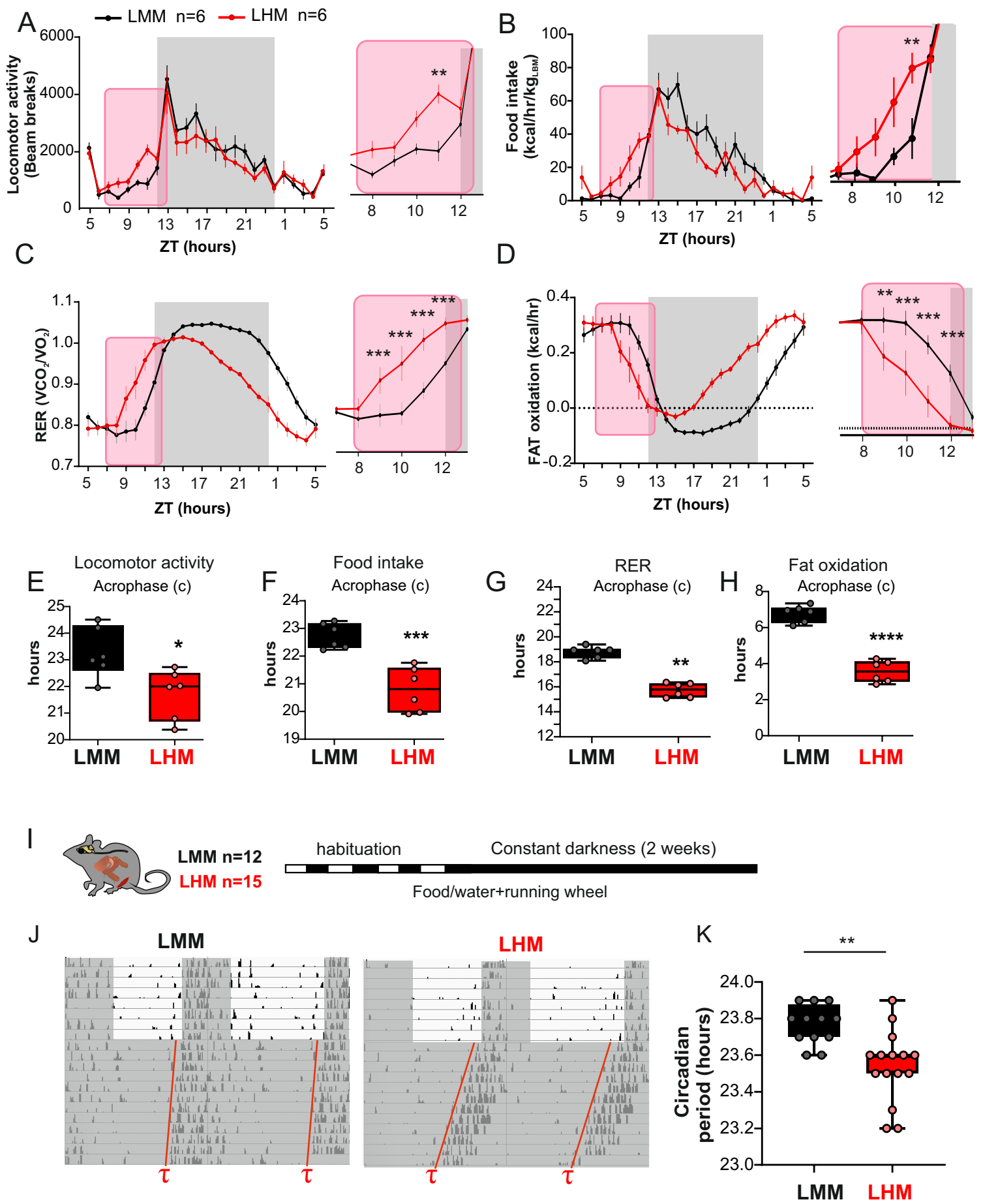


Figure 4

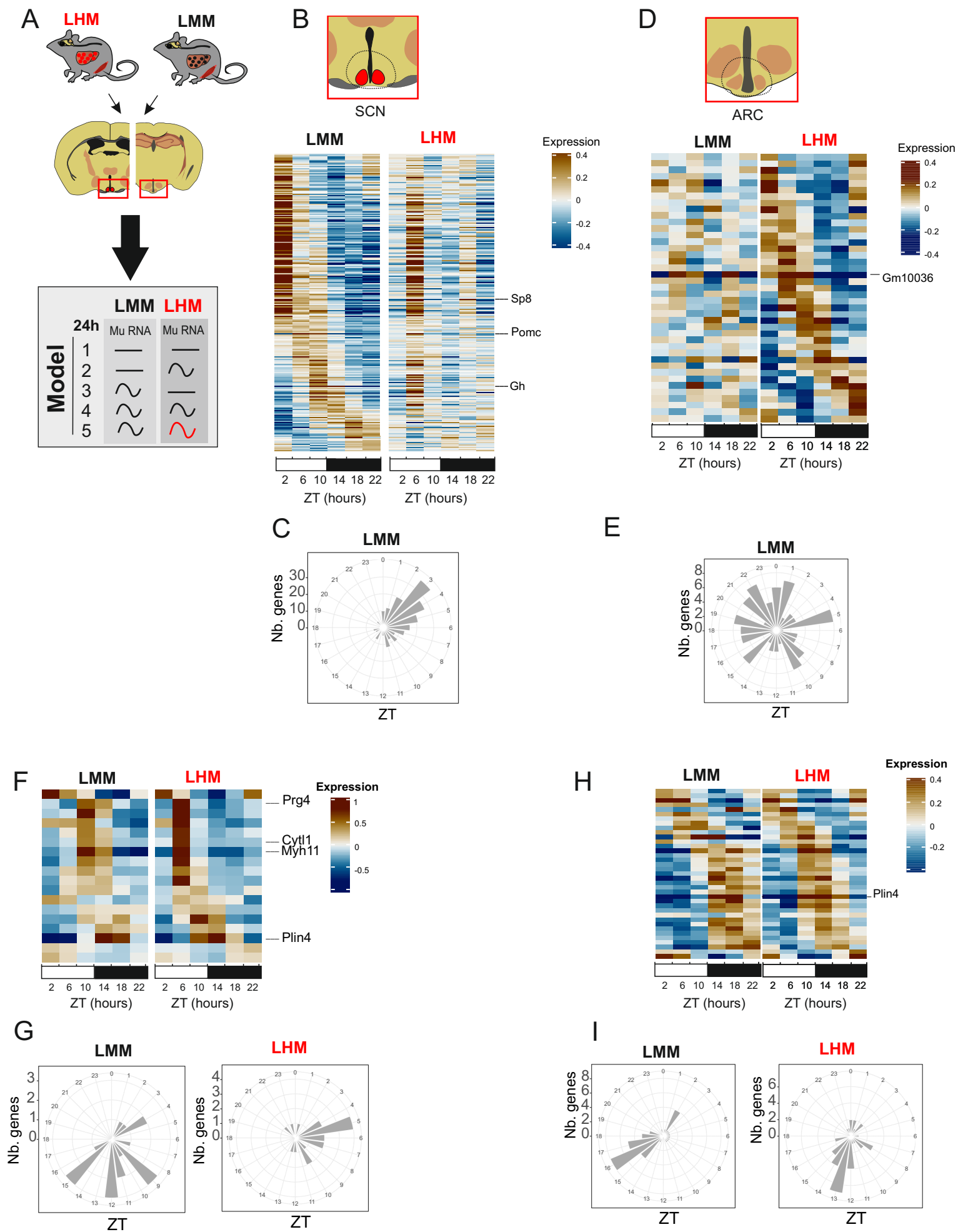


Figure 5

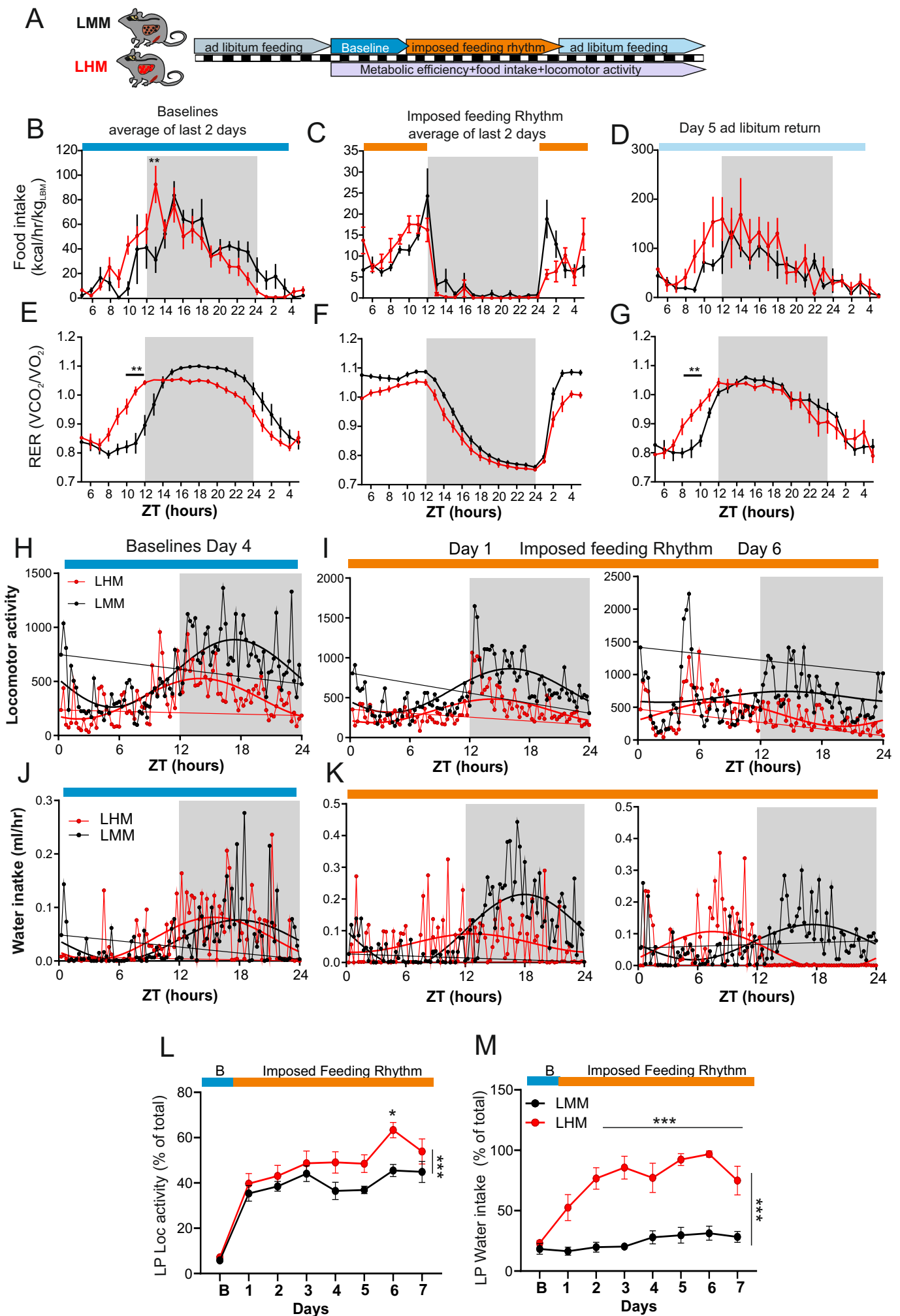


Figure 6